Chapter 1
Metallic Nanostructures: Fundamentals

Wenxin Niu and Xianmao Lu

Abstract This chapter focuses on the fundamental aspects of metallic nanostructures. We firstly introduce the definition, classification, and historical background of metallic nanostructures. A summary of their novel optical, catalytic, and magnetic properties is provided in the next section. General methods for the synthesis of metallic nanostructures are then outlined, followed by the discussion of their morphological, structural, and compositional characterization methods. Finally, representative examples for controlled syntheses of metallic nanostructures are highlighted.

1.1 Metallic Nanostructures: General Introduction and Historical Background

1.1.1 General Introduction

Nanoscience has emerged as one of the most exciting areas of modern science and technology. The development of nanoscience has revolutionized many applications ranging from catalysis to electronics, photonics, information storage, biological imaging and sensing, as well as energy conversion and storage [1–5]. Among these advances, metallic nanostructures have played a major role in many directions and have become one of the most studied subjects in nanoscience [6]. Metallic nanostructures are defined as metallic objects with at least one dimension in the range of one to a few hundred of nanometers. They exhibit many remarkable chemical and physical properties that are different from both individual metal atoms and bulk metals. The emergence of these novel properties is the driving force for the rapid development of research in metallic nanostructures, which has been on the forefront of scientific disciplines including chemistry, physics, materials science, medicine, and biology.

X. Lu (✉) · W. Niu
Department of Chemical and Biomolecular Engineering, National University of Singapore, 4 Engineering Drive 4, Singapore 117585, Singapore
e-mail: chelxm@nus.edu.sg

Y. Xiong, X. Lu (eds.), *Metallic Nanostructures,* DOI 10.1007/978-3-319-11304-3_1

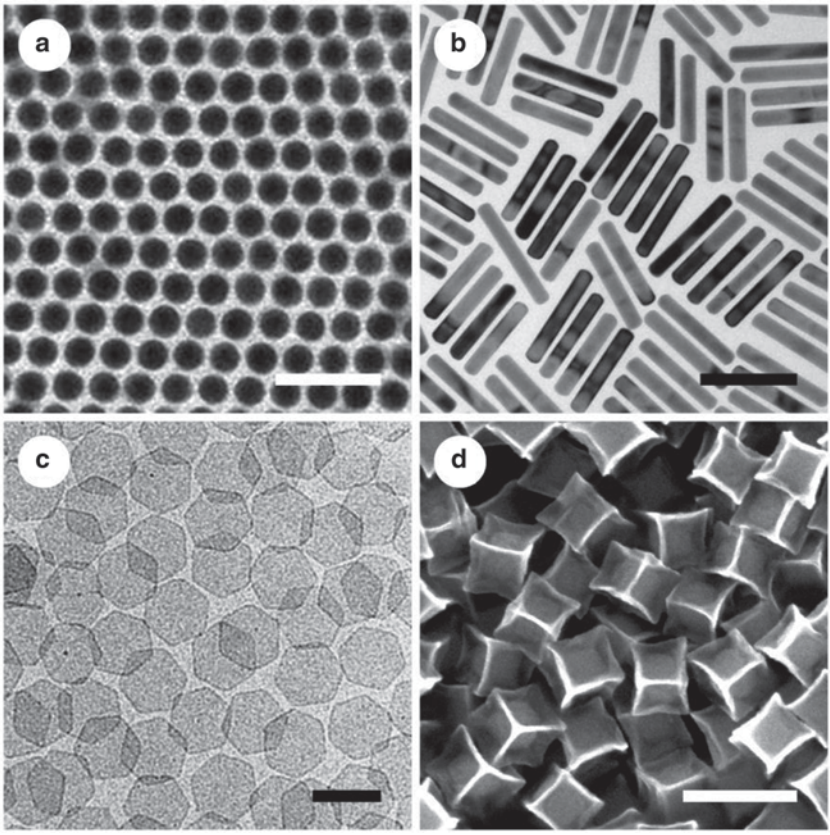

Fig. 1.1 Metallic nanostructures of different dimensions: **a** 0D Pd spherical nanoparticles (scale bar: 20 nm, reproduced with permission from reference [7], Copyright 2010 Wiley-VCH), **b** 1D Au nanorods (scale bar: 100 nm, reproduced with permission from reference [8], Copyright 2012 American Chemical Society), **c** 2D Pd ultrathin nanosheets (scale bar: 100 nm, reproduced with permission from reference [9], Copyright 2011 Nature Publishing Group), and **d** 3D Pd concave nanocubes (scale bar: 200 nm, reproduced with permission from reference [10], Copyright 2014 American Chemical Society)

1.1.2 Classification of Metallic Nanostructures

A typical way of classifying metallic nanostructures of different morphologies is to identify them according to their dimensions. Based on the number of dimensions, metallic nanostructures can be roughly classified as zero-dimensional (0D), one-dimensional (1D), two-dimensional (2D), and three-dimensional (3D). 0D metallic nanomaterials include small clusters composed of a few to roughly a hundred metal atoms, and common spherical metal nanoparticles. Figure 1.1a shows an example of 0D Pd spherical nanoparticles [7]. 1D metallic nanomaterials are nanostructures with large aspect ratios such as nanorods, nanowires, nanobelts (nanoribbons), and

Fig. 1.2 The dichroism of the Lycurgus cup: **a** viewed in transmitted light, **b** viewed in reflected light (from reference [20], Copyright Trustees of the British Museum), **c** medieval stained glass from Chartres Cathedral (from reference [21], Copyright Dr Stuart Whatling)

nanotubes. Figure 1.1b shows an example of 1D Au nanorods [8]. 2D nanomaterials are thin films with nanometer thickness such as nanosheets, nanoplates, and nanoprisms. Figure 1.1c shows an example of Pd ultrathin nanosheets with a thickness of 1.8 nm [9]. 3D nanomaterials include more complicated structures such as various polyhedra, as well as assemblies of 0D, 1D, and 2D nanostructures. Figure 1.1d shows an example of 3D Pd concave nanocubes with sub-10 nm sharp edges [10].

1.1.3 Historical Background of Metallic Nanostructures

Metallic nanostructures have been unknowingly used for a few purposes dating back for millennia. Gold and silver nanoparticles have been incorporated into glasses as colorant for over 2000 years [3]. One of the most well-known examples is the Lycurgus cup from the Roman times [11]. The Lycurgus cup has a remarkable characteristic of dichroism: the glass appears a color of green jade under normal external lighting conditions, while it gives a deep ruby red color when it is lighted from within (Fig. 1.2a, b). Modern transmission electron microscopy (TEM) studies proved that the fascinating colors originate from alloy nanoparticles of Ag and Au with sizes of 50–100 nm embedded in the glass [12]. When viewed in reflected light, the green color of the cup is due to the scattering contribution of the alloy nanoparticles [13]. When it is illuminated from inside, the color is resulted from the absorption contribution: the green wavelength is absorbed and the light that goes through the glass appears with the complementary red color.

In the Middle Ages, Au, Ag, and Cu nanoparticles have been frequently employed as colorants, particularly for church windows and pottery [14, 15]. In the seventeenth century, Andreas Cassius et al. described a procedure that can produce Au nanoparticles with an intense purple color [16]. This so-called "Purple of Cassius" was used to color glasses and produce the so-called "gold ruby glass" [17]. The preparation of "Purple of Cassius" involved the dissolution of gold metal in aqua regia followed by the reduction of Au(III) by a mixture of stannous chloride,

although the true chemical reaction mechanisms were not understood at that time [18]. Figure 1.2c shows a medieval-stained glass from Chartres Cathedral, in which the red color originates from Au nanoparticles. Ag and Cu nanoparticles were also dispersed in the glassy matrix of the ceramic glaze for luster decoration of medieval and Renaissance pottery [19].

The first documented scientific study of metal nanoparticles was performed by Michael Faraday [22, 23]. In 1857, Faraday reported that colloidal Au nanoparticles can be prepared by the reduction of gold salts with reagents including organic compounds or phosphorus [24]. Faraday's Au nanoparticles, with size between 3 and 30 nm, are still stable now [25]. Faraday correlated the red color of Au colloid with the small size of the Au particles in metallic form. He concluded that it is gold present in solution in a "finely divided metallic state" smaller than the wavelength of visible light that shows colors different from the original color [24]. Faraday also examined the synthesis of other metal nanoparticles such as Pt, Pd, Rh, and Ag [24].

Zsigmondy and Svedberg also made significant contributions to the development of metallic nanostructures [26]. Zsigmondy employed an ultramicroscope to study the optical properties of Au nanoparticles [27, 28]. He developed a method for preparing colloidal Au nanoparticles by boiling gold chloride with formaldehyde [27]. He even used small Au particles as nuclei for the growth of large Au nanoparticles, which is possibly one of the first seed-mediated growth methods for metallic nanostructures [27]. Svedberg also studied the synthesis of metal nanoparticles extensively [29]. He explored many reducing agents to produce Au nanoparticles from chloroauric acid, ranging from gas phase reductant hydrogen, hydrogen sulphide, and carbon monoxide (CO), to various organic and inorganic reducing agents [29]. In addition, he invented the ultracentrifuge, which allowed size separation of nanoparticles [30].

The revolutionary development of TEM enabled researchers to directly explore the morphology of metallic nanostructures [31]. In 1937, Beischer et al. first studied the shapes of Au nanoparticles using a TEM [32]. Since then, researchers have been able to correlate the sizes and shapes of metallic nanostructures with their synthetic conditions. In 1951, Turkevich et al. developed a method for producing spherical Au nanoparticles via citrate reduction of tetrachloroauric acid [33]. The citrate reduction method is very simple and can give Au nanoparticles with narrow size distribution. In 1973, Frens refined Turkevich's work and discovered that the size of Au nanoparticles can be simply controlled by tuning the ratio between sodium citrate and gold salt [34]. The citrate reduction method is still one of the most simple and reproducible approaches in synthesizing Au nanoparticles with controlled size. Besides TEM, the invention of numerous characterization and analytical technologies has greatly simulated the developments of modern research in metallic nanostructures [35]. Based on these high-resolution chemical and physical analyses, elucidation of structure–function relationships in metallic nanostructures has become possible. Morphology-controlled synthesis of metallic nanostructures has achieved unprecedented progress, even at atomic precision [36]. Many rational synthetic methods for metallic nanostructures have been developed and "materials by design" has become a goal of research in this area.

Table 1.1 Calculated sizes of cuboctahedral Pt nanoparticles and their corresponding surface atom percentages (reproduced with permission from reference [37], Copyright 2012 Wiley-VCH)

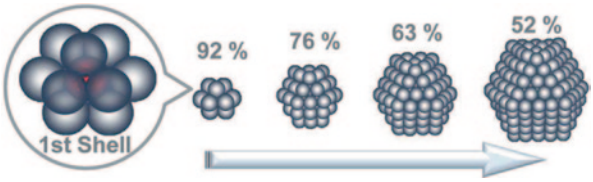

Number of shells	Number of surface atoms	Number of total atoms	Percentage of surface atoms (%)	Size of Pt nanoparticles (nm)
1	12	13	92	0.8
2	42	55	76	1.4
3	92	147	63	1.9
4	162	309	52	2.4
5	252	561	45	3.0
6	362	923	39	3.5
7	492	1415	35	4.1
8	642	2057	31	4.6
9	812	2869	28	5.1

1.2 Fundamental Properties of Metallic Nanostructures

The fast development in the synthesis of metallic nanostructures with controllable morphologies has enabled the discovery of their new properties [38]. Now it is well-known that size and shape of metallic nanostructures can profoundly alter their properties. One of the most well-known size-dependent properties of metallic nanostructures is their high surface area to volume ratio. Table 1.1 shows the relationships between particle size versus the percentage of surface atoms for Pt nanoparticles with cuboctahedral shapes [37]. It can be clearly seen that as the size of Pt nanoparticles decreases, a dramatic increase in the surface atom percentages can be obtained. The large surface area to volume ratio of metallic nanostructures is the origin of a number of unique applications, especially in catalysis [39]. Besides their sizes, the shape of metallic nanostructures also strongly affects their optical, catalytic, and magnetic properties. In this section, the correlation between these properties and the morphology of metallic nanostructures is briefly introduced.

1.2.1 Optical Properties

The brilliant colors of Au and Ag nanostructures have fascinated people for thousands of years. These phenomena arise from localized surface plasmon resonance (LSPR). LSPR is the resonant collective oscillation of free electrons of metallic

Fig. 1.3 Metallic nanostructures with tunable localized surface plasmon resonance (LSPR): **a** Au nanorods with different aspect ratios, **b** Au nanoshells with different shell thickness, and **c** Au/Ag nanocages with different composition and shell thickness (reproduced with permission from reference [40], Copyright 2012 The Royal Society of Chemistry)

nanostructures under light irradiation [41–43]. LSPR can result in strong light absorption, scattering, and enhanced local electromagnetic field. Based on these characteristics, plasmonic nanostructures have found broad application in biological sensing and imaging, photothermal therapy, and solar energy harvesting [43–46]. Metallic nanostructures possessing LSPR in visible wavelength range are usually metals with a negative real and small positive imaginary dielectric constant such as gold, silver, and copper [41]. One remarkable feature of LSPR is that its frequency and intensity are strongly dependent on the size, shape, and composition of the plasmonic metallic nanostructures. This provides an important method to tailor the LSPR of metallic nanostructures by synthetically tuning their structural parameters. For example, Fig. 1.3 shows three types of metallic nanostructures with tunable LSPR properties: nanorods, nanoshells, and nanocages [40, 47, 48]. Their optical properties can be controlled by tuning the aspect ratio, shell thickness, and composition. Another feature of LSPR is that it is very sensitive to the refractive index of the surrounding medium [41]. Pronounced red shifts in the LSPR spectral position can be observed when the refractive index of the surrounding medium increases. Based on this property, LSPR has been used for ultra-sensitive sensing [49].

1.2.2 Catalytic Properties

The rapid development of metallic nanostructures has impacted the field of heterogeneous catalysis considerably [51–54]. Metallic nanostructures with well-defined sizes and shapes can be a new family of model systems for establishing structure–function relationships in heterogeneous catalysis [55]. In conventional catalysis, the detailed crystal structure and crystallographic facets of metallic nanocatalysts are usually not well resolved. However, these structural parameters can have a dramatic effect on their catalytic activity. A typical example is the discovery of Au catalysts in low-temperature CO oxidation [56, 57]. Although bulk Au is very unreactive for

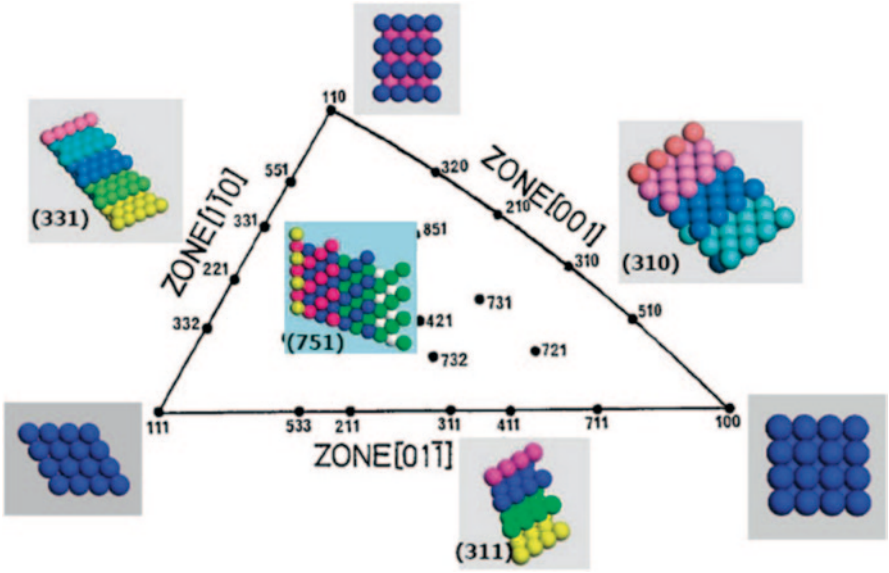

Fig. 1.4 Unit stereographic triangle of face-centered cubic (fcc) metal single-crystal and models of surface atomic arrangement (reproduced with permission from reference [50], Copyright 2008 American Chemical Society)

low-temperature CO oxidation, Au nanoparticles in sizes of 3–4 nm are catalytically active for this reaction. The advance in metallic nanostructures now allows one to control their size, shape, and composition precisely, offering new opportunities to discover cost-effective and active metallic catalysts [58]. For instance, by controlling the surface crystal facets of Pt nanocrystals, their catalytic activity can be significantly increased [59]. Figure 1.4 shows the surface atomic arrangements of various crystal facets of face-centered cubic (fcc) metals [50]. Pt nanostructures with high-index facets can exhibit up to 400% increase in catalytic activity for the electrooxidation of small organic fuels compared with common Pt catalysts [60]. The activity is attributed to the open structure with a high density of unsaturated atoms on the high-index facets. The selectivity of catalytic reaction can also be control by the shape of metallic nanostructures [37]. Somorjai et al. showed that during the benzene hydrogenation reactions, cyclohexane and cyclohexene products were formed on cuboctahedral Pt nanocrystals with both {111} and {100} facets, whereas, only cyclohexane was produced on Pt nanocubes enclosed by {100} facets [61].

1.2.3 Magnetic Properties

The size and shape of ferromagnetic metal nanostructures have a significant impact on their magnetic properties [62]. Superparamagnetism is one of the most interesting phenomena arising from the shrinking size of metallic nanostructures. In metallic nanostructures of a critical size, the thermal energy is sufficient to invert

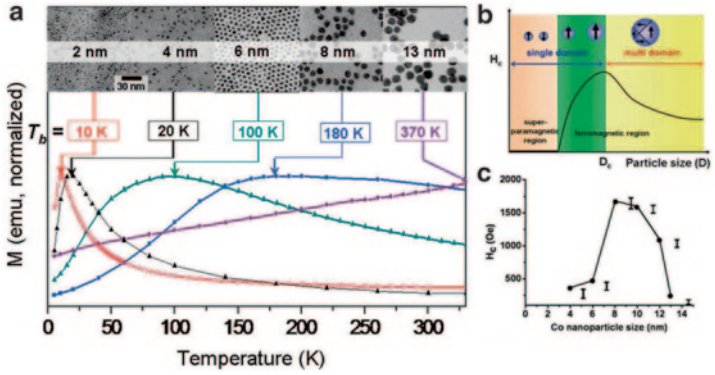

Fig. 1.5 **a** Zero-field cooling curves and transmission electron microscopy (TEM) images of Co nanoparticles with sizes of 2, 4, 6, 8, and 13 nm. **b** Size-dependent magnetic domain structures from superparamagnetism to single domain and multidomain ferromagnetism. **c** Size-dependent coercivity of Co nanoparticles (reproduced with permission from reference [62], Copyright 2008 American Chemical Society)

the magnetic spin direction and the magnetic fluctuation results in a net magnetization of zero. This phenomenon is called superparamagnetism [63]. Apparently, the transition from ferromagnetism to superparamagnetism is temperature dependent and this transition temperature is referred as the blocking temperature [64]. The blocking temperature of metallic nanostructures is strongly dependent on their sizes. In the case of cobalt nanoparticles, ferromagnetic to superparamagnetic transitions of nanoparticles with sizes of 2, 4, 6, 8, and 13 nm occur at 10, 20, 100, 180, and 370 K, respectively (Fig. 1.5a) [65]. The magnetic coercivity of cobalt nanoparticles is also dependent on their sizes. For Co nanoparticles with single magnetic domain structures, the magnetic coercivity increases with the size of the nanoparticles. For Co nanoparticles with multiple magnetic domains, the magnetic coercivity decreases as the size of the Co nanoparticles increases (Fig. 1.5b and c) [66]. The magnetic coercivity of metallic nanostructure is also dependent on their shape and composition [67–69]. For example, Co nanowires with high aspect ratios have a much higher coercivity than those with small aspect ratios [67].

1.3 General Methods for the Synthesis of Metallic Nanostructures

The quest for methods of producing metallic nanostructures with controllable sizes and morphologies has been always a challenging subject. The interest in rationally synthesizing metallic nanostructures with controllable sizes and morphologies is not based solely on their esthetic appeal. The sizes and morphologies of metallic nanostructures will play a pivotal role in determining their properties [42, 52, 70–72]. Therefore, the ability to generate metallic nanomaterials with well-controlled

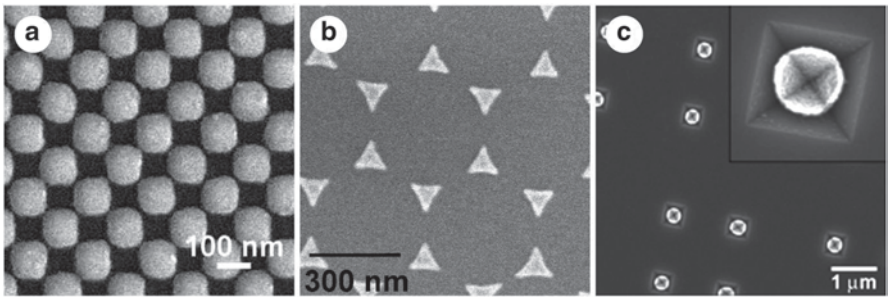

Fig. 1.6 Metallic nanostructures fabricated by combining physical vapor deposition and nanofabrication methods: **a** A checkerboard cluster of Au nanoblocks separated by nanogaps through electron beam lithography (reproduced with permission from reference [79], Copyright 2011 American Chemical Society), **b** An array of triangular copper nanostructures by nanosphere lithography (reproduced with permission from reference [88], Copyright 2007 American Chemical Society), **c** Pyramidal Au nanostructures supported on Si pedestals fabricated by templating Si wafer with etched holes (reproduced with permission from reference [89], Copyright 2005 American Chemical Society)

sizes, shapes, and compositions is central to unraveling the chemical and physical properties of metal nanostructures. Since the time of Faraday, numerous approaches have been developed to control the morphology and composition of metallic nanostructures. Besides simple chemical reduction or thermal decomposition routes, various techniques such as thermal evaporation, laser ablation, and electrochemical, photochemical, sonochemical processes have been developed. These methods could be realized either through chemical or physical processes in gas, liquid, or solid phases.

1.3.1 Gas- and Solid-Phase Methods

Many gas-phase synthesis approaches are based on physical vapor deposition (PVD), in which metallic nanostructures are generated through homogeneous or heterogeneous nucleation and growth through a vapor of metal atoms. A few techniques can be used to evaporate metals, such as arc discharge [73], laser ablation [74], ion sputtering [75], electron beam [76], or simply thermal evaporation [77]. However, most of these methods can only produce metallic nanomaterials with broad size distribution and usually have limited control on their morphology. Combined PVD with nanofabrication methods such as electron beam lithography can generate 2D metallic nanostructures with arbitrary sizes and shapes, although the throughput may be low (Fig. 1.6a) [78, 79]. Besides lithographic methods, templates can also be used to produce nanostructures with anisotropic shapes [80, 81]. For example, Van dyne et al. has developed a technique called nanosphere lithography to fabricate arrays of metallic nanostructures (Fig. 1.6b) [82]. This method uses close-packed sphere arrays of monodispersed polystyrene or silica nanospheres as templates for the deposition of truncated triangular prisms of different metals. By templating against a

single-crystal Si wafer with an array of etched holes, Odom et al. were able to generate free-standing pyramidal metallic nanostructures with diameters down to 80 nm and curvatures of tip radii as small as 2 nm (Fig. 1.6c) [81].

An alternative gas phase synthesis approach is chemical vapor deposition (CVD). In a typical CVD process, a substrate is exposed to one or more volatile precursors of metallic nanostructures, then the precursors may react or decompose on the substrate surface to produce corresponding metal nanostructures [83]. A popular variation of CVD is atomic layer deposition (ALD) [84]. ALD has emerged as an important technique for depositing metallic thin films and supported metallic nanoparticles with controllable size, composition, and structures [85]. During ALD processes, metallic nanostructures are grown via sequential, self-limiting chemical reactions between precursor vapors and the substrate surface [86]. There are only a finite number of surface sites on the substrate surface, therefore, only a finite number of surface species can be deposited [87]. Precise control over metal nanoparticle size, composition, and structure can be achieved by manipulating the combination of ALD sequence, surface treatment, and deposition temperature [84].

Most PVD and CVD processes start at the molecular level to build up metallic nanostructures. Conversely, metallic nanostructures can be produced from bulk metals through top-down approaches. For example, solid-phase mechanical processes such as grinding and milling have been used to reduce the size of metal materials into nanoscale [90, 91]. Nanoscale metallic powders are produced by high-energy ball milling of bulk materials. Colloidal stabilizers or supports are commonly added during the grinding and milling processes to avoid the aggregation of metal nanoparticles during the size reduction processes.

1.3.2 Wet Chemical (Liquid Phase) Methods

Gas- and solid-phase methods have advantages in obtaining nanomaterials with high purity and some of the processes are readily applicable to large-scale production. However, size and morphology control of metallic nanostructures are difficult to achieve with these methods if they are not combined with nanofabrication techniques. In addition, some of the techniques require high vacuum and expensive instruments. In contrast, synthetic methods based on wet chemistry have received intense attention and exhibit a few advantages over gas- and solid-phase methods [72, 92–94]. Wet chemical methods have greater flexibility and versatility in synthesizing metal nanostructures with controlled size, shape, and composition. For wet chemical methods, different reaction parameters such as precursor, surfactant, shape-directing agent, and reaction temperature can be independently manipulated. Moreover, wet chemical methods are easier to scale up and there is no need for expensive equipment. Over the past 30 years, many wet chemical methods have been developed for metallic nanostructures [72]. Most of these methods inevitably involve the precipitation of metals into solid phase in solution through chemical reduction or decomposition. In the following sections, a few wet chemical methods are introduced. These methods vary from common chemical reduction and ther-

mal decomposition, to hydrothermal and solvothermal reactions at high pressure, synthetic processes involving microwave heating, radiation, electrochemistry, sonochemistry, syntheses at interfaces and in reversed micelles, and syntheses directed by templates.

1.3.2.1 Chemical Reduction and Thermal Decomposition

Chemical reduction is the most traditional method for metallic nanostructures [95, 96]. It has been successfully applied in synthesizing noble metal nanostructures such as Au, Ag, Pd, Rh, and Pt [72]. In a typical chemical reduction process, several regents are essential in addition to metal salts. The first one is the reducing agent, which donates electrons and reduces the metal salts to metal atoms. Important reducing agents include sodium borohydride, hydrazine, hydroxylamine, hydrogen, CO, and organic compounds such as sodium citrate, various sugars, alcohols, aldehydes, amides, and amines [26, 96]. To avoid the aggregation of metal nanostructures, a stabilizing agent is generally needed [97]. Stabilizing agents are usually surfactants or polymers that can be absorbed to the surface of metal nanostructures. To achieve morphology control, some shape-directing agents might be added. These shape-directing agents may have specific interactions with certain facets of the metal nanostructures or can change the reduction kinetics and induce the anisotropic growth of the nanostructures [92]. These agents include atomic/ionic species such halides [98, 99] and metal ions [100], surfactants [97], polymers [101], or biomolecules such as peptides [102–106].

Salts of reactive metals such as Fe, Co, and Ni have relatively low reduction potentials and cannot be reduced with common reducing agents. In these cases, thermal decomposition of their organometallic compounds becomes an attractive route for the synthesis of these metallic nanostructures [107, 108]. A typical thermal decomposition process usually involves the hot injection of an organometallic precursor into a heated solvent in the presence of suitable stabilizing agent [109]. Various metal nanoparticles including Fe, Ni, Co, as well as their alloys have been prepared through thermal decomposition [109–111]. It should be noted that CO generated from the decomposition of metal carbonyl precursors also has a strong effect on the shape evolution of metal nanostructures [112].

The synthesis of metallic nanostructures with narrow size distribution and uniform morphology has long been a great challenge [72, 92, 93, 113, 114]. To achieve this goal, the nucleation step must be separated from the growth step during the synthesis of metallic nanostructures, thus simultaneous secondary nucleation and growth can be avoided. Therefore, it is necessary to induce a single nucleation event in the nucleation step. This could be realized through a hot-injection method, in which a quick injection of metal precursor into hot reducing solvent could yield a fast nucleation process [115, 116]. An alternative and possibly better approach is seed-mediated growth [117, 118]. Seed-mediated growth is a typical heterogeneous nucleation process, which involves the synthesis of metal nanoseeds and the growth of the seeds in another growth solution. The seeds can catalyze the reduction of

metal salts by reducing agents, therefore, they can continually grow into large nanostructures and the secondary nucleation can be efficiently discouraged. Therefore, a better control over size and shape of metallic nanostructures can be attained. Moreover, seed-mediated method is promising in identifying shape-directing agents and providing mechanistic insight into the growth mechanisms of metal nanostructure due to its high controllability [119, 120].

1.3.2.2 Hydrothermal and Solvothermal Method

For common chemical reduction or thermal decomposition methods in solution phase, the reaction temperatures generally cannot exceed the boiling points of the solvents. Under hydrothermal and solvothermal conditions, the reactions are proceeded in a sealed container and water or solvents can be heated to temperatures above their boiling points [127–129]. In the meantime, heating can increase the autogenous pressure in the reaction container, causing significantly increased reactivity of the reducing agents and precursors [130, 131]. There have been many successful examples using hydrothermal and solvothermal processes to synthesize metallic nanostructures. For example, different Ag nanocrystals including nanocubes, right bipyramids, nanorods, nanospheres, and nanowires can be produced through cetyltrimethylammonium bromide (CTAB)-modified silver mirror reactions at hydrothermal conditions [132, 133]. Pd nanowires have been synthesized in high yields through an iodide-assisted hydrothermal process (Fig. 1.7a) [121]. Solvothermal methods have been especially successful to synthesize noble metals such as Pt and Pd (Fig. 1.7b). A few Pd, Pt, and their alloy nanostructures with high surface energy have been synthesized [134–139]. Under hydrothermal and solvothermal conditions, small adsorbates with low boiling point can be effectively introduced to control the growth of metal nanostructures [140].

1.3.2.3 Microwave Method

Microwave can be used as an energy source to heat reaction solutions and induce the reduction of metal salts or the decomposition of metal complexes into metallic nanostructures [141, 142]. Under microwave irradiation, polar molecules such as H_2O and polyols tend to orientate with the external electric field from microwave. When dipolar molecules try to re-orientate with alternating high-frequency electric fields, molecular friction between the polar molecules will generate heat [143]. Compared with normal heating methods such as heating using oil bath and heating mantle, microwave methods provide rapid, uniform, and efficient heating of reagents and solvents [144, 145]. The rapid and uniform heating can promote the reduction of metal precursors and the nucleation of metal clusters, leading to the formation of nanostructures with uniform sizes. Besides the common heating effect, hot spots may be created on the solid–liquid surfaces when metal nanostructures are heated by microwave [141]. Upon microwave heating, the adsorption of surfactant with a

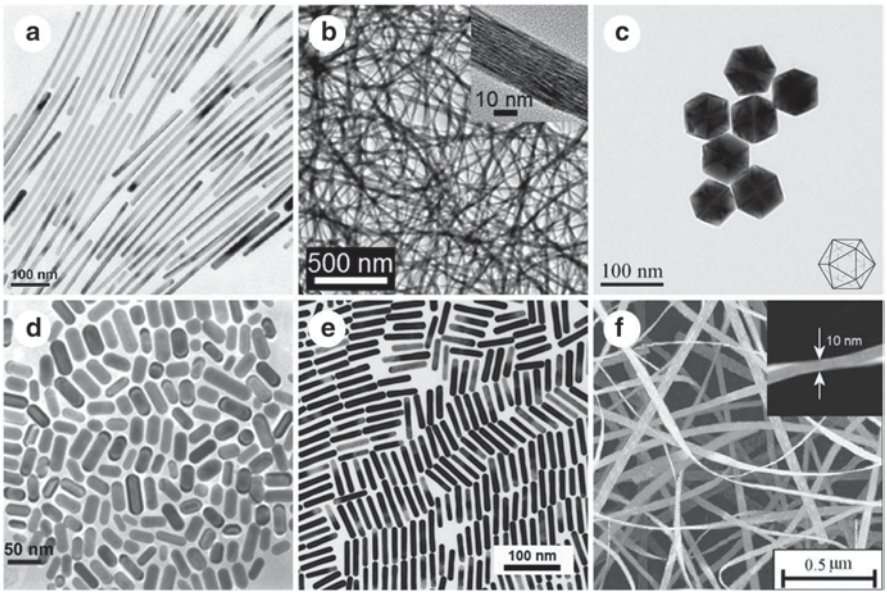

Fig. 1.7 Metallic nanostructures synthesized with different wet chemical methods: **a** Pd nanowires via hydrothermal method (reproduced with permission from reference [121], Copyright 2009 American Chemical Society), **b** Pt nanowire bundles via solvothermal method (reproduced with permission from reference [122], Copyright 2013 American Chemical Society), **c** Pd icosahedral nanocrystals via microwave method (reproduced with permission from reference [123], Copyright 2009 International Union of Pure and Applied Chemistry), **d** Au nanorods via photochemical method (reproduced with permission from reference [124], Copyright 2002 American Chemical Society), **e** Au nanorods via electrochemical method (reproduced with permission from reference [125], Copyright 1998 American Chemical Society), **f** Au nanobelts via sonochemical method (reproduced with permission from reference [126], Copyright 2006 Wiley-VCH)

large dielectric loss constant on metal nanostructures can create hot surfaces on solid metals, and this could be a specific shape-control strategy not attainable by other methods. For example, Liu and Huang et al. have applied microwave irradiation to synthesize uniform Pd icosahedral and cubic nanocrystals (Fig. 1.7c) [123, 146, 147].

1.3.2.4 Radiolytic and Photochemical Method

Radiolytic reduction can be employed as a powerful tool to produce metallic nanostructures [148]. Normal ionization radiations such as electron beam, X-ray, gamma-ray can cause the formation of hydrated electrons, OH^*, and H^* radicals during radiolysis of aqueous solutions [149, 150]. These species can cause the reduction of metal salts. Ultra-violet (UV) light, on the other hand, can also cause the formation of radicals through photolysis reactions. For example, Au nanorods were obtained after a solution containing acetone irradiated with a 254-nm UV light. Radicals are generated via the excitation of acetone by UV light and cause the

reduction of gold salts (Fig. 1.7d) [124]. The aspect ratio of the final rods can be simply tuned by the amount of silver ions added to the system [151].

Visible light can also be involved in the synthesis of metallic nanostructures [152]. This process is mainly based on the plasmonic properties of noble metal nanostructures. Upon the excitation the plasmonic modes of Au or Ag nanostructures, visible light can induce the shape transformation of metal nanocrystals. Mirkin, Xia et al. discovered a photo-induced method for converting small Ag nanoparticles into nanoprisms, nanoplates, and nanobelts [153–156]. For Ag nanoprisms, edge lengths in the 30–120 nm range can be controlled by using dual-beam illumination of the Ag nanoparticles [155]. The process is believed to be driven by surface plasmon excitations. The plasmon excitations may cause the photo-oxidation of citrate by hot "holes" from plasmon dephasing on the surface of Ag nanostructures, oxidative etching of Ag in the presence of oxygen, and selective reduction of aqueous Ag ions to form larger nanoprisms [157].

1.3.2.5 Electrochemical Method

Electrochemical process was employed as a synthesis method of metallic nanostructures almost 100 years ago by Svedberg [29]. Reetz et al. further developed this method in recent years to synthesize metal nanoparticles [158, 159]. Their process generally is based on a two-electrode setup. The sacrificial anode consists of a bulk metal is transformed into metal nanoparticles upon electrochemical treatment. In 1997, the electrochemical method was successfully used to synthesize single-crystalline Au nanorods with tunable aspect ratios (Fig. 1.7e) [125, 160]. Recently, electrochemical methods have also been applied to synthesize metal nanostructures with defined crystal facets [50]. Sun et al. pioneered the synthesis of platinum, palladium, rhodium, and iron nanocrystals with high-index facets and unconventional shapes using electrochemical method [50]. Repetitive adsorption/desorption of oxygen generated by square-wave potential are believed to play a key role in the formation of high-index facets. Oxygen atoms preferentially adsorb at high-index facets because high-index facets contain many step atoms with low coordination numbers. Therefore, high-index facets are preserved during the electrochemical treatment [59].

1.3.2.6 Sonochemical Method

Ultrasound has also been used as a unique tool for the synthesis of metallic nanostructures in recent years [161, 162]. A few metallic nanostructures, such as Au clusters, Ag nanoprisms, Au nanorods, dodecahedra, octahedral, and belt-like nanostructures (Fig. 1.7f) have been synthesized by using sonochemical methods [126, 163–168]. The effect of ultrasonic radiation on chemical reactions arises from a phenomenon called acoustic cavitation. Acoustic cavitation involves the formation, growth, and implosive collapse of bubbles in a liquid [169]. The transient temperature and pressure in and around the collapsing bubbles can reach as high as

5000 K and 1800 atm. Moreover, the heating and cooling rates are extremely high, which is in the order of 10^{10} K/s [170]. The extreme temperature and pressure and high energy produced during acoustic cavitation can cause the reduction or decomposition of metal precursors and lead to the formation of metallic nanostructures in a room-temperature liquid phase, eliminating the requirement of high temperatures, high pressures, or long reaction times [171]. Ultrasonic irradiation treatment of volatile precursor and non-volatile precursors follows different mechanisms. For volatile precursors such as organometallic compounds, free metal atoms will be generated by bond dissociation due to the high temperatures created during bubble collapse [170]. In the case of non-volatile precursors, ultrasonic irradiation of water can generate highly reactive H^* and OH^* radicals, which are strong reducing agents for the chemical reduction of metal salts. Moreover, these reactive radicals can further react with organic species in the solution and generate secondary radicals (R^*) [172]. The secondary radicals can dramatically promote the reduction rate of metal salts. Metallic nanoparticles synthesized with volatile organometallic compounds are generally amorphous, while metallic nanostructures produced from non-volatile precursors are usually well crystallized [161].

1.3.2.7 Reversed Micelle Method

Reverse micelles are defined as globular aggregates formed through the self-assembly of surfactants in apolar solvents [173]. A reverse micelle has a polar core and an apolar shell, which are formed by the assembly of the hydrophilic heads and the hydrophobic chains of the surfactants, respectively [174]. Water confined in the polar cores of reverse micelles are separated as many water-in-oil droplets, which act as effective nanoreactors for the growth of metallic nanostructure with tailored size, shape, and composition [175]. By modulating water to surfactant ratio, the droplet size of reverse micelles can be readily tuned in the nanometer range. An important feature of reverse micelles is that the water-in-oil droplets are not kinetically stable and a dynamic exchange process is occurring between different colliding droplets [176]. Based on this characteristic, the synthesis of metallic nanostructure in reverse micelles can be achieved by mixing two reverse micelle solutions containing hydrophilic metal salts and reducing agents, respectively [177]. After mixing, the droplets collide and exchange the metal salts and reducing agents, leading to the nucleation and growth metallic nanostructures in the water-in-oil droplets. The synthesis of metallic nanostructure in reverse micelle systems has proved to be effective for monodisperse metal nanoparticles [178, 179].

1.3.2.8 Multiphase Process

Interfaces play an important role in the nucleation and growth of metallic nanostructures [180]. By carefully designing the chemical reactions taking place at the interfaces of different phases, better control over the size and shape of metallic

nanostructures can be achieved. A well-known example is the broadly used Brust–Schiffrin method [181]. The Brust–Schiffrin method is especially useful for the synthesis of ultra-small gold clusters and nanoparticles with small diameters [182]. Because of the utilization of thiols as stabilizing agents, the as-formed Au nanoparticles can be selectively functionalized and have a much better stability [183]. The nanoparticles can be repeatedly isolated and redispersed in common organic solvents without aggregation. The typical Brust–Schiffrin procedure involves three major steps: (1) phase transfer of gold species from an aqueous solution to the organic phase assisted by a long-chain quaternary ammonium surfactant; (2) reduction of Au(III) to Au(I) by thiols; and (3) reduction of Au(I) to Au(0) by a strong reducing agent such as sodium borohydride [184].

Li et al. developed a liquid–solid–solution phase transfer and separation strategy to synthesize monodispersed metal nanoparticles [185]. When aqueous solutions of noble metal salts, sodium linoleate, linoleic acid, and ethanol were mixed, three phases would form: an upper liquid phase of ethanol and linoleic acid, a middle solid phase of sodium linoleate, and a bottom solution phase of noble metal salts in water and ethanol mixed solvent. During the reaction, metal ions will enter the solid phase and form metal linoleate through ion exchange. Then ethanol could reduce the noble metal ions at the liquid–solid or solution–solid interfaces. The formed metal nanoparticles can be stabilized by in situ generated linoleic acid. Finally, the hydrophobic metal nanoparticles could be collected at the bottom of the reaction container. This method can be generalized to synthesize various noble metal nanoparticles, including Ag, Ru, Rh, Ir, Au, Pd, and Pt.

1.3.2.9 Template-Based Syntheses

Many of the previously introduced methods can only produce 0D or polyhedral metallic nanostructures with isotropic shapes. Forming anisotropic metallic nanostructures through symmetry breaking is especially challenging for metallic nanostructures because most metals possess highly symmetric crystal lattices [186]. Therefore, there are only limited strategies to control the morphology of anisotropic metallic nanostructures, such as judiciously control over the reaction conditions, selection of shape-direction agents, manipulation of growth kinetics, or formation of specifically twinned structures [187–191]. Synthesis using a pre-existing nanostructured template is an alternative and effective strategy that can achieve high degree of morphology control, especially for highly anisotropic metallic nanostructures [192, 193]. Many types of nanomaterials can be considered as templates to direct the growth of metallic nanostructures. Most of them can be classified into three major categories: soft templates, hard templates, and sacrificial templates.

Soft matters such as polymers and biological molecular assemblies can be used as templates for the growth of metallic nanostructures. For example, Crooks et al. developed a method using dendrimers as templates for the synthesis of metal nanoparticles [200]. After sequestering metal ions within dendrimers, corresponding metal nanoparticles can be synthesized through chemical reduction.

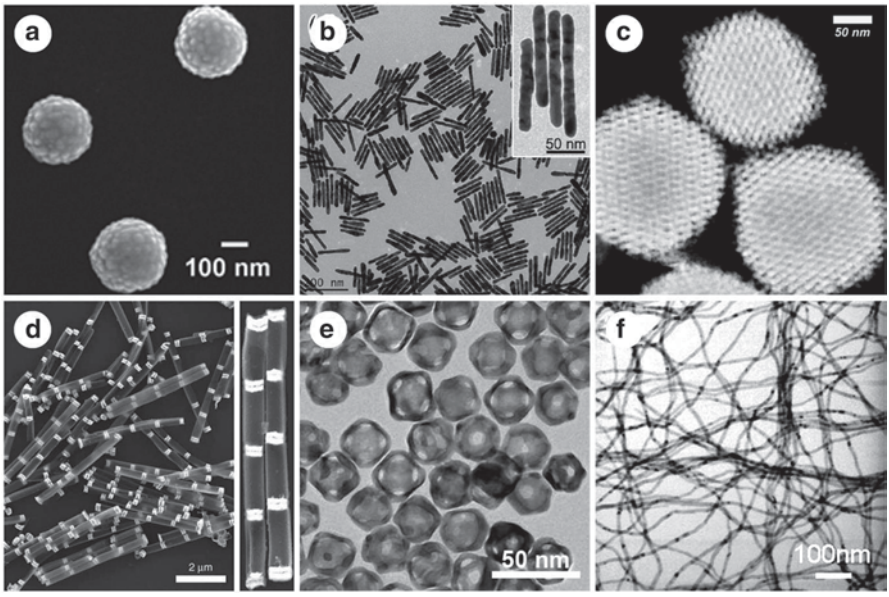

Fig. 1.8 Metallic nanostructures synthesized with template-based methods: **a** Au nanoshells with silica spheres as templates (reproduced with permission from reference [194], Copyright 2005 American Chemical Society), **b** Au nanorods with silica nanotubes as templates (reproduced with permission from reference [195], Copyright 2011 American Chemical Society), **c** mesoporous Pt nanostructures with 3D mesoporous silica as templates (reproduced with permission from reference [196], Copyright 2011 American Chemical Society), **d** metal nanostructures with controllable gaps via on-wire lithography (reproduced with permission from reference [197], Copyright 2009 Nature Publishing Group), **e** Au/Ag nanocages with Ag nanocubes as sacrificial templates (reproduced with permission from reference [198], Copyright 2013 The Royal Society of Chemistry), **f** Pt nanowires with tellurium nanowires as sacrificial templates (reproduced with permission from reference [199], Copyright 2009 Wiley-VCH)

The uniform structure of dendrimer templates allows for the generation of metal nanoparticles with uniform sizes. The dendrimer-encapsulated metal nanoparticles have a substantial fraction of unpassivated surface and may have a higher catalytic activity than common metal nanoparticles. By using lamellar bilayer membranes as 2D templates, ultrathin single-crystalline Au nanosheets were obtained in confined water layers [201, 202].

Soft templates usually have a limited effect on the shapes of the metallic nanostructures. In contrast, hard templates with specific structures have a profound effect of the as-obtained metallic nanostructures. By using silica spheres as templates, Halas et al. were able to fabricate Au nanoshells with tunable optical properties [194, 203]. To coat the silica spheres with Au nanoshells, small Au nanoparticles were first attached to the silica cores by using linker molecules. Then more gold was deposited onto the seeds until the seed nanoparticles coalesced into a complete shell (Fig. 1.8a) [204]. By varying the diameters of the silica sphere templates and the thickness of the nanoshell, the optical resonance of Au nanoshells can be

systematically tuned over a broad region ranging from visible to the mid-infrared [205]. By using a similar seeding technique, Yin et al. synthesized various noble metal nanorods in silica nanotube templates [195]. Silica nanotubes can confine the growth of metal nanostructures and form a metal nanorod@silica core-shell structure. Silica can be easily etched to release dispersed metal nanorods (Fig. 1.8b). 3D mesoporous silica has also been used as templates for the growth of mesoporous metallic nanostructures (Fig. 1.8c) [196, 206, 207].

Channels in porous membranes were also employed as 1D hard templates for the synthesis of metallic nanostructures [208]. By using chemical or electrochemical methods, metal can be deposited into channels of the porous templates, after removal of the templates, nanotubes, or nanowires of a wide range of materials can be obtained [209]. Two types of porous membranes are commercially available: ion-track-etched membranes and anodic aluminum oxide (AAO) templates [210, 211]. Based on AAO templates, Mirkin et al. further developed a technique called on-wire lithography for synthesizing metallic nanostructures with controllable gaps (Fig. 1.8d) [197, 212]. They first used electrochemical deposition to prepare segmented nanowires composed of a noble metal and a sacrificial metal. After the removal of the template and deposition of a backing material on the segmented nanowires, the sacrificial metal layers can be selectively etched, leaving noble metal nanostructures with controllable gaps. The gap size is controlled by the thickness of the sacrificial metal layer [213].

Besides serving solely as templates, sacrificial templates can be also involved in chemical transformations during the synthesis of metallic nanostructures. Templates can function as reducing agents and lead to the deposition of metal on their surfaces. For example, Xia et al. employed galvanic replacement reactions to synthesize various hollow metal nanostructures (Fig. 1.8e) [214]. Ag nanostructures can be used as sacrificial templates for generating hollow nanostructures of Au, Pt, Pd, and Ag alloys [198]. Many pre-synthesized nanostructures can act as reducing agents for metal ions. For example, selenium and tellurium nanowires have been used as both reducing agent and sacrificial templates for noble metal and their alloy nanowires/nanotube (Fig. 1.8f) [199, 215]. Hollow metal nanocages have been synthesized with Cu_2O nanocrystals as templates, in which Cu_2O was oxidized into Cu(II) species while metal salts were reduced to metallic cages [216, 217].

1.4 Characterizations of Metallic Nanostructures

1.4.1 Techniques for Morphological Analysis

1.4.1.1 Transmission Electron Microscope

TEM is one of the most useful and straightforward microscopic methods to characterize the morphologies of metallic nanostructures [222]. It can be directly utilized to visualize the size, shape, structure, and dispersity of metallic nanomaterials.

TEM operates on similar working principles as the light microscope, except that TEM uses an electron beam instead of light to probe the samples. Electron beams can exhibit wavelengths that are 10,000 times smaller than those of visible light, which makes it possible to get a much better resolution using TEM [223]. In TEM, the high energy electron beam is collimated and focused by electrostatic and electromagnetic lenses, and transmitted through the sample [224]. The transmitted electron beam is magnified and focused by an objective lens and appears on the imaging screen. A more detailed schematic comparison between the structures of TEM and the light microscope can be found in the book by Bozzola and Russell [225]. High-resolution transmission electron microscope (HRTEM) has allowed the imaging of samples with resolutions below 0.5 Å (with magnifications more than 50 million times) [226]. Therefore, HRTEM can determine the position of atoms and defects of the samples, and the locations of atoms and grain boundaries can be rigorously interrogated and examined [227]. Figure 1.9a–d shows HRTEM of metal

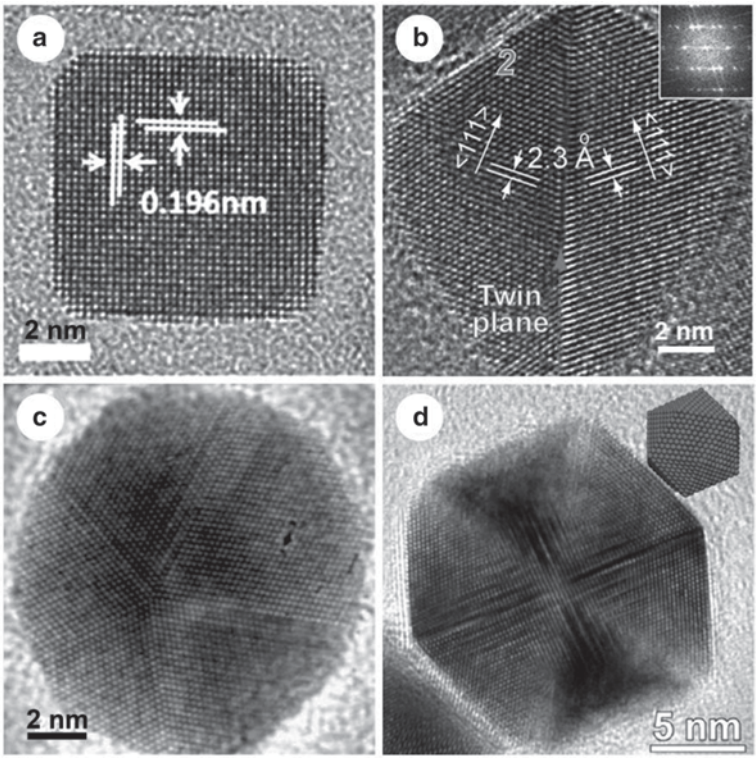

Fig. 1.9 High-resolution transmission electron microscope (HRTEM) images of metal nanoparticles with different crystal structures: **a** single-crystalline Pt nanocubes (reproduced with permission from reference [218], Copyright 2012 American Chemical Society), **b** single-twinned Pd bipyramids (reproduced with permission from reference [219], Copyright 2013 American Chemical Society), **c** penta-twinned Au nanoparticles (reproduced with permission from reference [220], Copyright 2006 The Royal Society of Chemistry), **d** icosahedral multiply twinned Pt nanoparticles (reproduced with permission from reference [221], Copyright 2013 American Chemical Society)

nanostructures with four typical crystal structures: single-crystalline Pt nanocubes [218], single-twinned Pd bipyramids [219], penta-twinned Au nanoparticles [220], and icosahedral multiply-twinned Pt nanoparticles [221], respectively.

1.4.1.2 Scanning Electron Microscope (SEM)

SEM is one of the most versatile instruments available for the examination and analysis the 3D morphology of metallic nanostructures [228]. It produces images of a sample by scanning it with a focused beam of electrons. The electrons interact with the atoms in the sample and produce various signals that contain information about the sample's surface morphology and composition [229]. To study the topographic feature of a sample, the secondary electron operation mode of SEM is commonly used, which collects the inelastically scattered electrons. When a sample is scanned with an electron beam, the secondary electrons can only escape from a thin layer near surface of the sample, therefore, the surface topography information of the sample can be provided [230]. Although the resolution of the SEM is lower than that of the TEM, it has very large depth of field and can image a bulk sample of several centimeters in size with 3D representation. By using electron beams generated with a field emission gun, it is possible to achieve up to 900 K magnification for SEM imaging [231]. Figure 1.10 shows several examples using SEM to study the assembly behaviors of Ag and Au nanostructures [8, 232, 233].

1.4.1.3 Atomic Force Microscope (AFM)

AFM is a type of scanning probe microscopy techniques for examining the surface of materials [234]. AFM can provide a direct 3D visualization of materials. Qualitative and quantitative information on the size, morphology, and surface roughness can be obtained accordingly. AFM provides the information of the topography of the sample by measuring the atomic force between the atoms at the surface of the sample and the AFM tip [235]. During the operation of AFM, a tip at the end of a cantilever is scanned across the sample surface, and the forces between the tip and the surface cause the cantilever to deflect, providing data to form images for the surface of the sample [236]. AFM can provide measurements of ultrathin nanomaterials with a vertical resolution of less than 0.1 nm with XY resolution of approximately 1 nm [237]. Figure 1.11b shows an AFM image of ultrathin Rh nanosheets [137]. Based on AFM measurement, the thickness of the Rh nanosheets is only 0.4 nm. Compared with SEM, AFM can be operated in ambient air and liquid environment. A major drawback of AFM is the limited area that it can scan: typically, AMF can only scan samples on the order of micrometer [238].

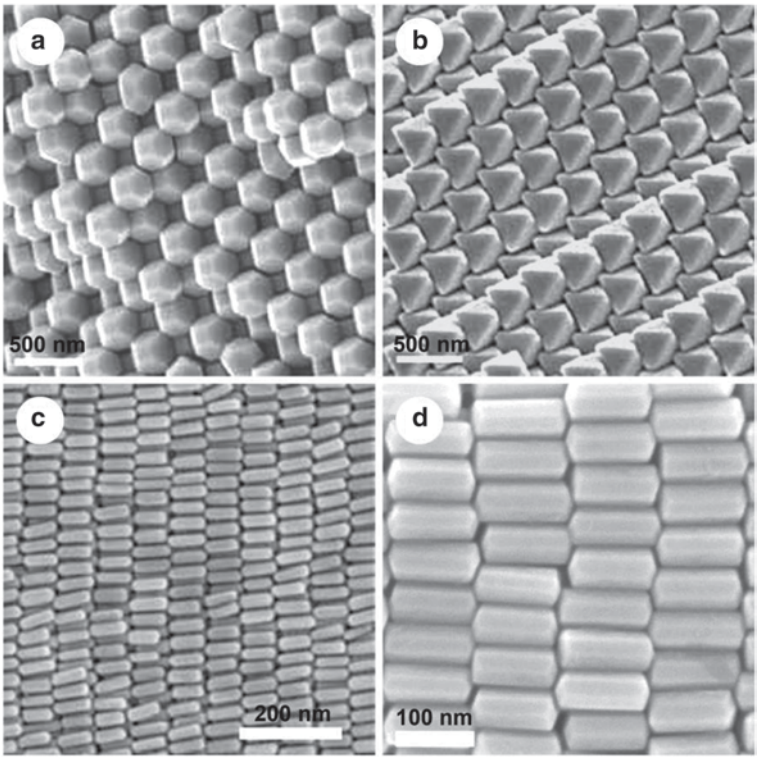

Fig. 1.10 Scanning electron microscopy (SEM) images of assemblies of metal nanostructures: **a** and **b** Ag truncated octahedral nanocrystals and Ag octahedral nanocrystals, respectively (reproduced with permission from reference [232], Copyright 2012 Nature Publishing Group); **c** and **d** Au nanorods with different aspect ratios (reproduced with permission from reference [8] and [233], Copyright 2012 and 2013 American Chemical Society)

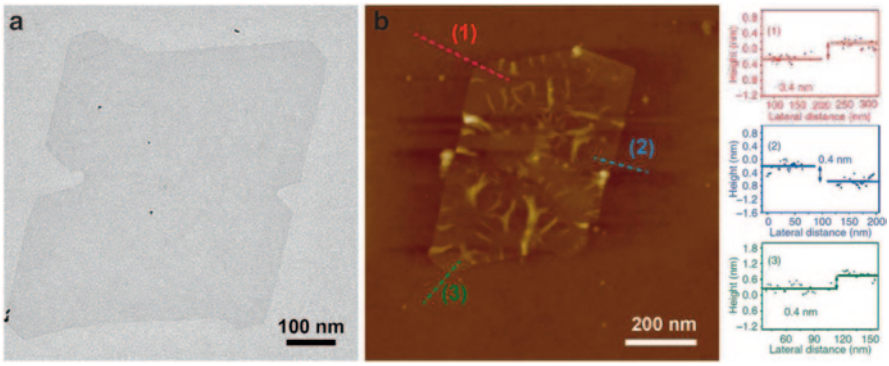

Fig. 1.11 Transmission electron microscopy (TEM) image, atomic force microscopy (AFM) image, and the corresponding height profiles of ultrathin Rh nanosheets (reproduced with permission from reference [137], Copyright 2014 Nature Publishing Group)

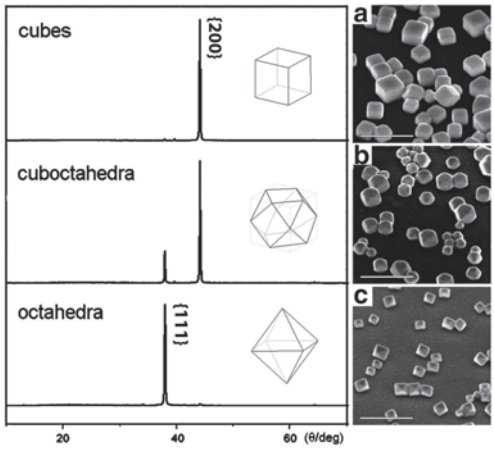

Fig. 1.12 X-ray diffraction patterns and corresponding scanning electron microscopy images of Au nanocrystals with different shapes: **a** cubes, **b** cuboctahedra, **c** octahedra (reproduced with permission from reference [242], Copyright 2006 American Chemical Society)

1.4.2 Techniques for Crystal Structural Analysis

1.4.2.1 X-Ray Diffraction (XRD)

XRD is a non-destructive technique to characterize the crystallographic structure, grain size, and preferred orientation in solid samples [239]. Powder diffraction is commonly used to identify unknown crystalline substances. It may also be used to characterize heterogeneous solid mixtures to determine the relative abundance of crystalline materials [238]. During XRD testing, a monochromatic X-ray directed onto a sample and the interaction between X-rays and different crystal planes of the sample will lead to the diffraction of X-rays [240]. By recording the scattered intensity of the X-ray beam as a function of incident and scattered angle, a spectrum will be obtained. Two types of fingerprint information of a particular crystalline material are provided in the spectrum: the peak positions (corresponding to lattice spacing according to Bragg's law) and the relative intensity of the peaks [231]. XRD is also useful in size measurement of structural nanocrystalline materials using Scherrer equation. The Scherrer equation is a formula that relates the size of sub-micrometer crystallites to the broadening of a peak in a diffraction pattern [241]. It can determine the size of crystalline nanoparticles in powder samples. XRD is capable of investigating the structural information of metal nanocrystals. For example, Fig. 1.12 shows the XRD patterns and corresponding SEM images of Au nanocrystals with different shapes [242]. When the shapes of Au nanocrystals gradually evolved from cubes with {100} facets to octahedra with {111} facets, their XRD patterns also show the decrease of {200} peaks and the increase of {111} peaks.

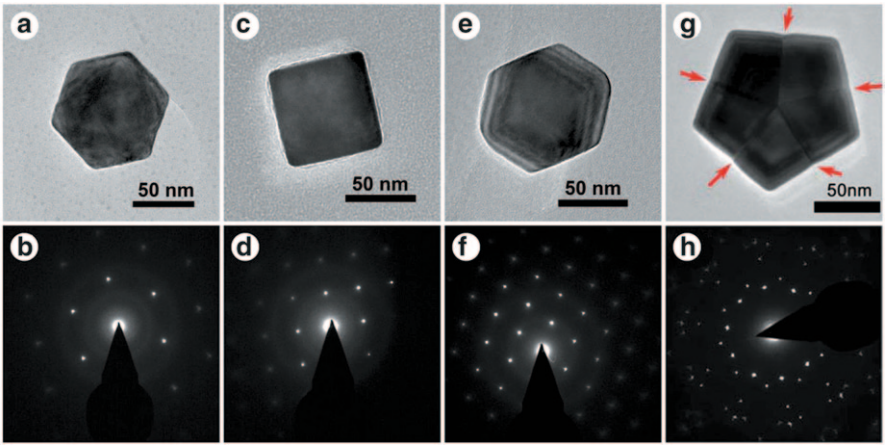

Fig. 1.13 Transmission electron microscopy images and corresponding selected area electron diffraction patterns of different metallic nanostructures: **a**, **b** an octahedral Pd nanocrystal recorded along the [$\bar{1}$11] zone axis; **c**, **d** a cubic Pd nanocrystal recorded along the [001] zone axis; **e**, **f** a rhombic dodecahedral Pd nanocrystal recorded along the [011] zone axis (reproduced with permission from reference [247], Copyright 2010 American Chemical Society); and **g**, **h** a penta-twinned Au nanocrystal recorded along the [011] zone axis (reproduced with permission from reference [248], Copyright 2013 The Royal Society of Chemistry)

1.4.2.2 Selected Area Electron Diffraction (SAED)

SAED is a crystallographic experimental technique that usually coupled with TEM microscopes for microanalysis [243]. Unlike XRD, which can only provide crystallographic structure of bulk samples, SAED can provide crystallographic information on the single nanostructure level. SAED analysis can reveal whether a material is polycrystalline, single-crystalline, or amorphous. A crystalline material will produce a diffraction pattern composed of several spots. The center spot is associated with the non-diffracted transmitted electron beam, whereas all the other spots are diffracted spots [244]. These diffraction spots represent the beams diffracted from different sets of planes. The distance between the diffraction spots and center spot is $1/d_{hkl}$, where d_{hkl} is the interplanar spacing between (hkl) planes [245]. If the sample is polycrystalline, in which individual crystal domains are oriented in different directions, the diffraction pattern is the overlap of diffraction spots from each individual crystal domain. Small crystal size and large numbers of crystals will lead to the formation of continuous diffraction rings [246]. Figure 1.13a–f show the TEM images and corresponding SAED patterns of single-crystalline octahedral, cubic, and rhombic dodecahedral Pd nanocrystals, respectively [247]. Their characteristic diffraction patterns are indicative of their crystal facets of {111}, {100}, and {110}, respectively. In Fig. 1.13g and h, a SAED pattern of a penta-twinned Au nanocrystal along the [110] direction is shown [248]. The penta-twinned Au nanocrystal is formed by five single crystals with {111} twin planes as indicated in Fig. 1.13g. The diffraction pattern can be interpreted by superimposing the [110] SAED pattern of each crystal rotated by 72° with respect to each other [220].

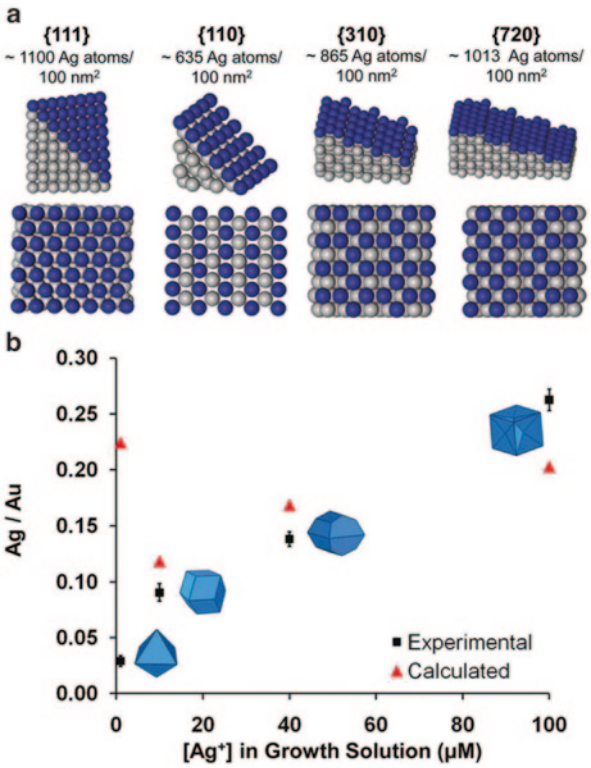

Fig. 1.14 X-ray photoelectron spectroscopy (XPS) analysis of Ag adsorption on Au nanocrystals with different crystal facets: **a** models of Ag atoms adsorbed on different Au facets (*Blue spheres* represent surface atoms), **b** Ag/Au ratio for each facets obtained from XPS data (*black*), and theoretical values for monolayer coverage of Ag based on models in (**a**). (reproduced with permission from reference [253], Copyright 2011 American Chemical Society)

1.4.3 Techniques for Composition Analysis

1.4.3.1 X-ray Photoelectron Spectroscopy (XPS)

XPS is a spectroscopic technique to analyze the materials within several nanometers from the surface [249]. XPS is an important analytical technique that can probe the chemical state and chemical composition of a sample. XPS can detect elements with atomic number larger than 3, with parts per million detection limit [226]. During XPS measurement, the system is irradiated with a monochromatic X-ray beam to promote the emission of photoelectrons of the surface atoms [2]. The emitted photoelectrons are then collected and analyzed using an electron spectrometer. XPS spectra are recorded by plotting the number of photoelectrons escaped from the surface of the sample versus the binding energy. The binding energy of the emitted photoelectrons can be calculated from the energy of the incident beam and the measured kinetic energy of the electrons [250]. The chemical shifts in the binding energies of the photoelectrons are indicative of the chemical states of the detected elements [251]. The short mean free path of the emitted electrons in solids makes XPS a surface-sensitive method to analyze the surface composition of metallic nanostructures [252]. For example, Mirkin et al. have used XPS to investigate the surface coverage of Ag atoms on different Au crystal facets and illustrate the function of Ag underpotential deposition in the synthesis of Au nanocrystals (Fig. 1.14) [253].

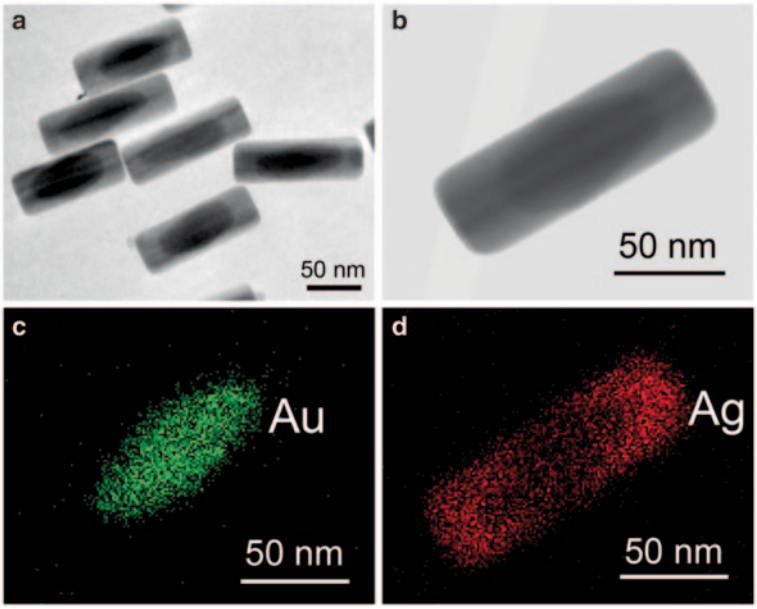

Fig. 1.15 **a**, **b** Transmission electron microscopy images of Au@Ag core-shell nanorods and **c**, **d** Energy-dispersive X-ray spectroscopy elemental mapping of Ag and Au for the Au@Ag nanorod shown in (**b**) (reproduced with permission from reference [257], Copyright 2013 Wiley-VCH)

1.4.3.2 Energy-Dispersive X-Ray Spectroscopy

Energy-dispersive X-ray spectroscopy (EDX, EDS, or EDAX) is an analytical technique used for the elemental analysis of a sample [254]. It is based on the analysis of characteristic X-ray lines from the sample when exposed with a beam of charged particles such as electron beams. Electron beams can remove an inner shell electron from the sample and create a vacancy. Then an electron of higher states fill the resulted vacancy and release the energy difference between these two states of electrons in the form of X-rays [255]. The number and energy of the X-rays emitted from a specimen are measured by an energy dispersive spectrometer. An EDX spectrum is a plot of intensity versus X-ray energy. The energy of emitted X-rays is distinctive characteristic of each element, therefore, the EDX spectra can be used to identify the composition and measure the quantity of elements in the sample [256]. EDX systems are most commonly found as a feature of SEM or TEM. Therefore, the composition analysis can be coupled with the morphology of the nanomaterials through different scanning modes such as spot, linear, or mapping scan. For example, EDX mapping has been used to study the structure of Au@Ag core-shell nanorods (Fig. 1.15) [257].

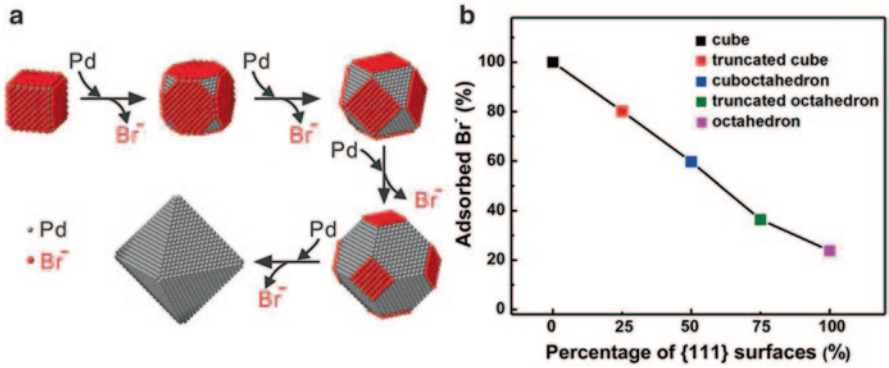

Fig. 1.16 **a** Schematic illustration for the processes of bromide ion desorption during the Pd overgrowth on Pd {100} surfaces, **b** inductively coupled plasma mass spectrometry analysis of the residual bromide ions at different growth stages, indicating that bromide ions desorbed from the Pd {100} surfaces during the Pd overgrowth (reproduced with permission from reference [264], Copyright 2013 American Chemical Society)

1.4.3.3 Inductively Coupled Plasma Atomic Emission Spectroscopy/Mass Spectrometry

Inductively coupled plasma atomic emission spectroscopy (ICP-AES, also called inductively coupled plasma optical emission spectrometry—ICP-OES) [258] and inductively coupled plasma mass spectrometry (ICP-MS) [259] are two of the most popular methods for quantitative elemental analysis of trace metals. Both techniques are based on inductively coupled plasma (ICP) techniques. ICP is a high temperature excitation source that can efficiently excite and ionize atoms [260]. Liquid samples are dried, vaporized, atomized, ionized, and finally transformed into a fine liquid aerosol after it travels through the plasma torch [261]. The excited atoms and ions that represent the elemental composition of the sample are ready to be quantified by atoms emission spectroscopy (AES) or mass spectrometry (MS). In the case of AES, the excited atoms and ions for a particular element emit electromagnetic radiation at characteristic wavelengths. The intensity of the radiation measured at specific wavelengths is proportional to the concentration of the corresponding element in the solution. Most elements can be quantitatively measured using ICP-AES with sensitivity down to parts per billion [262]. In ICP-MS, the sample is ionized with ICP and then the formed ions are separated and quantified by a mass spectrometer. The intensity of a specific peak in the mass spectrum is proportional to the amount of the element in the original sample. ICP-MS is capable of detecting metals and several non-metals at concentrations as low as part per trillion [263]. The ICP methods offer multi-element analytical capability within a broad dynamic range and good precision [261]. Xia et al. studied the bromide ion-assisted growth of Pd nanocrystals with ICP-MS. During the growth of Pd cubic seeds into cuboctahedra and then octahedra, the bromide ions are gradually released from the surface of Pd nanocrystals, as illustrated by the ICP-MS results in Fig. 1.16 [264]. This quantitative information can be used to estimate the amount

of bromide ions needed to generate Pd nanocrystals with {100} and {111} facets of desired ratios.

1.5 Representative Examples for Shape-Controlled Synthesis of Metallic Nanostructures

1.5.1 Seed-Mediated Growth Methods

Seed-mediated growth methods have been broadly used to control the sizes and morphologies of metallic nanostructures [117, 265]. In seed-mediated growth methods, the nucleation and growth stages of metallic nanostructures are well separated, therefore, a better control over the size distribution and morphology evolution of metallic nanostructures can be readily achieved [118–120]. The seeding strategy has been used to synthesize Au nanoparticles since the time of Zsigmondy [28]. In the 1990s, Brown and Natan developed a method to synthesize monodisperse Au nanoparticles based on Au nanoparticle-catalyzed reduction of Au salts by hydroxylamine [266–268]. They have described the observation of some rod-like Au nanostructures in their reports. However, it is until the year of 2001 when seed-mediated growth methods were rediscovered as an efficient strategy for controlling the morphologies of metallic nanostructures [269, 270]. The Murphy group first reported the synthesis of Ag and Au nanorods using seed-mediated growth methods with CTAB as a surfactant and ascorbic acid as a reducing agent. In the case of Au nanorods, they developed a three-step protocol that yielded long Au nanorods with penta-twinned structures (Fig. 1.17a) [270–272]. Although a high yield of Au nanorods could be achieved after shape separation, the actual purity of nanorods in the original products was only 5–10 % [273]. In 2002, the El-Sayed group developed an alternative seed-mediated approach to synthesize Au nanorods. By using single-crystalline Au nanoparticles as seeds and silver nitrate as a shape-directing agent, single-crystalline Au nanorods with high yields approaching 100 % were synthesized [274]. Moreover, by changing the amount of silver nitrate, the aspect ratio of Au nanorods could be tuned and this leads to tunable plasmonic properties. Subsequent studies have made a few variations of the initial reaction conditions of Au nanorods to achieve more control and better monodispersity (Fig. 1.17b) [275–279]. For example, the Wang group explored the effect of chain lengths of alkyl group of surfactants and was able to synthesize Au nanorods with very high aspect ratios [280, 281]. The Murray group has explored aromatic additives [8], binary surfactant mixture composed of CTAB and sodium oleate [282], and bromide-free surfactant composed of alkyltrimethylammonium chloride and sodium oleate for the synthesis of Au nanorods [233], respectively. These studies have achieved large-scale synthesis of Au nanorods with ultrahigh monodispersity and purity.

In 2004, another report from the Murphy group described the application of seed-mediated growth methods in synthesizing multiple shapes of Au nanostructures, such as rectangle-, hexagon-, cube-, triangle-, and star-like morphologies [283]. Shape control by manipulation of the kinetic and thermodynamic parameters of Au

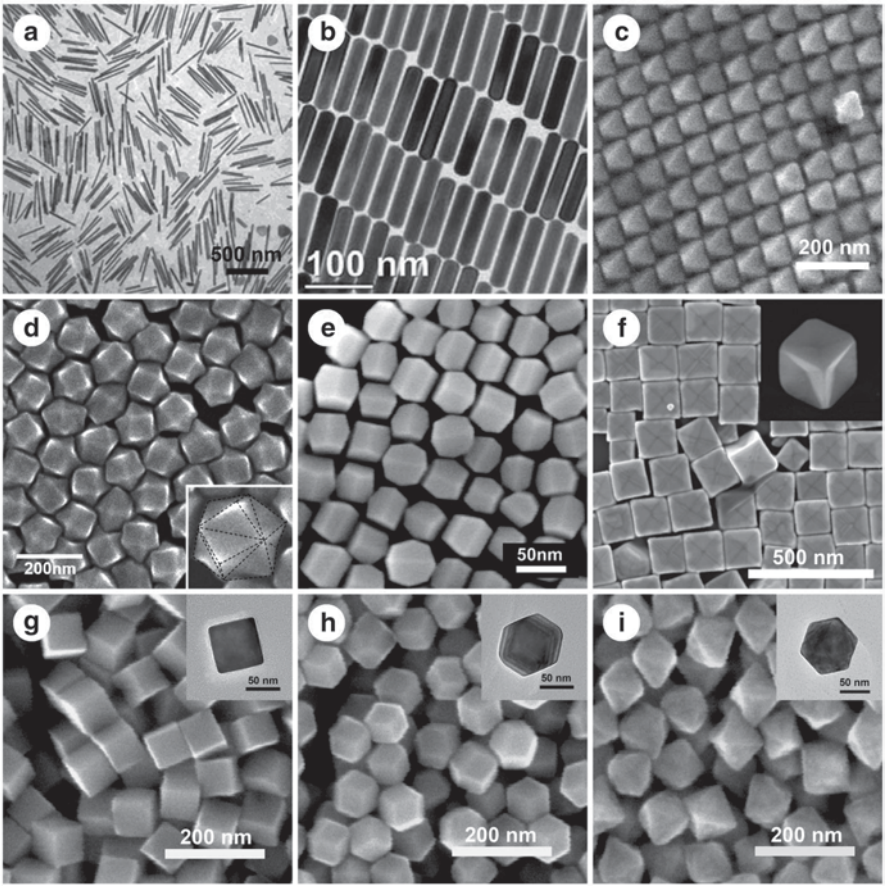

Fig. 1.17 Metallic nanostructures synthesized with seed-mediated growth methods: **a** penta-twinned Au nanorods via three-step growth (reproduced with permission from reference [272], Copyright 2004 American Chemical Society), **b** single-crystalline Au nanorods via Ag(I)-assisted growth (reproduced with permission from reference [282], Copyright 2013 American Chemical Society), **c** Au octahedra (reproduced with permission from reference [284], Copyright 2008 American Chemical Society), **d** Au trisoctahedral nanocrystals (reproduced with permission from reference [287], Copyright 2010 American Chemical Society), **e** Au truncated ditetragonal nanoprisms (reproduced with permission from reference [293], Copyright 2011 American Chemical Society), **f** concave Au nanocubes (reproduced with permission from reference [295], Copyright 2010 American Chemical Society), **g**–**i** Pd cubic, rhombic dodecahedral, and octahedra nanocrystals (reproduced with permission from reference [247], Copyright 2010 American Chemical Society)

nanostructures has received considerate attention since this study. The synthesis of a variety of Au nanostructures such as cubes, octahedra (Fig. 1.17c), rhombic dodecahedra, and trisoctahedra (Fig. 1.17d) has been rationalized by correlating their shapes and growth kinetics and thermodynamics [284–287]. In 2005, the function of silver nitrate in the synthesis of Au nanorods was revealed as an underpotential

deposition (UPD) mechanism [279]. The UPD of foreign metal atoms on metal nanostructures can stabilize high-energy facets and has been an important strategy to synthesize metallic nanostructures with high-energy facets [253, 288, 289]. Elongated tetrahexahedra with {730} facets [290], tetrahexahedra with {520} facets [291], rhombic dodecahedra with {110} facets [292, 293], truncated ditetragonal prisms with {310} facets (Fig. 1.17e) [293], hexagonal bipyramids with {210} facets [294], and concave cubes with {720} facets (Fig. 1.17f) [295] have been synthesized based on the UPD mechanism. UPD was also employed to control the architectural diversity of heterogeneous metallic nanostructures [296].

Seed-mediated growth methods have been successfully applied in synthesizing Pd and various core-shell metallic nanostructures [10, 247, 257, 297–306]. For example, rhombic dodecahedral, cubic, and octahedral Pd nanocrystals, as well as their derivatives with varying degrees of edge- and corner-truncation were synthesized through manipulation of the concentration of KI and the reaction temperature (Fig. 1.17g–i) [247]. Polyhedral Au@Pd core-shell nanocrystals including concave trisoctahedra with {hhl} facets, concave hexoctahedra NCs with {hkl} facets, and tetrahexahedra NCs with {hk0} facets were synthesized under careful control of their growth kinetics [303]. Au@Ag core-shell nanocrystals with cubic, truncated cubic, cuboctahedral, truncated octahedral, and octahedral shapes were synthesized by regulating the growth rates of different crystal facets [300].

1.5.2 The Polyol Process

The polyol process is one of the most versatile methods to synthesize metal nanostructures with controllable morphologies [72, 307]. Nanostructures of many different metals including Ag, Au, Pt, Pd, and Rh have been synthesized with polyol method [72]. In polyol processes, various polyols such as ethylene glycol, 1,5-pentanediol, di(ethylene glycol), and triethylene glycol are used as both the solvent and the reducing agent for the reduction of metallic precursors [187, 308, 309]. Polyvinylpyrrolidone (PVP) is commonly used as a stabilizing agent and sometimes a shape-directing agent for the growth of metallic nanostructures. The rapid development of the polyol process in the synthesis of metallic nanostructures dates back to the seminal report of polyol synthesis of Ag nanocubes by the Xia group in 2002 [310]. In the report, monodispersed Ag nanocubes were synthesized by reducing silver nitrate with ethylene glycol in the presence of PVP (Fig. 1.18a). In their subsequent studies, rational synthesis of Ag nanostructures was demonstrated by a mechanism called oxidative etching [311]. During the growth of Ag nanostructures, oxygen and halides can selectively remove Ag seeds with certain crystal structures. In the case of Ag nanocubes, twinned seeds can be removed by oxygen and chloride due to their high activity [312, 313]. Thus, a high yield of Ag nanocubes can be obtained. If the reaction was performed without oxidative etching, penta-twinned Ag nanowires can be synthesized (Fig. 1.18b) [314]. By using bromide and oxygen as a weaker etchant, single-twinned Ag right bipyramids were synthesized (Fig. 1.18c)

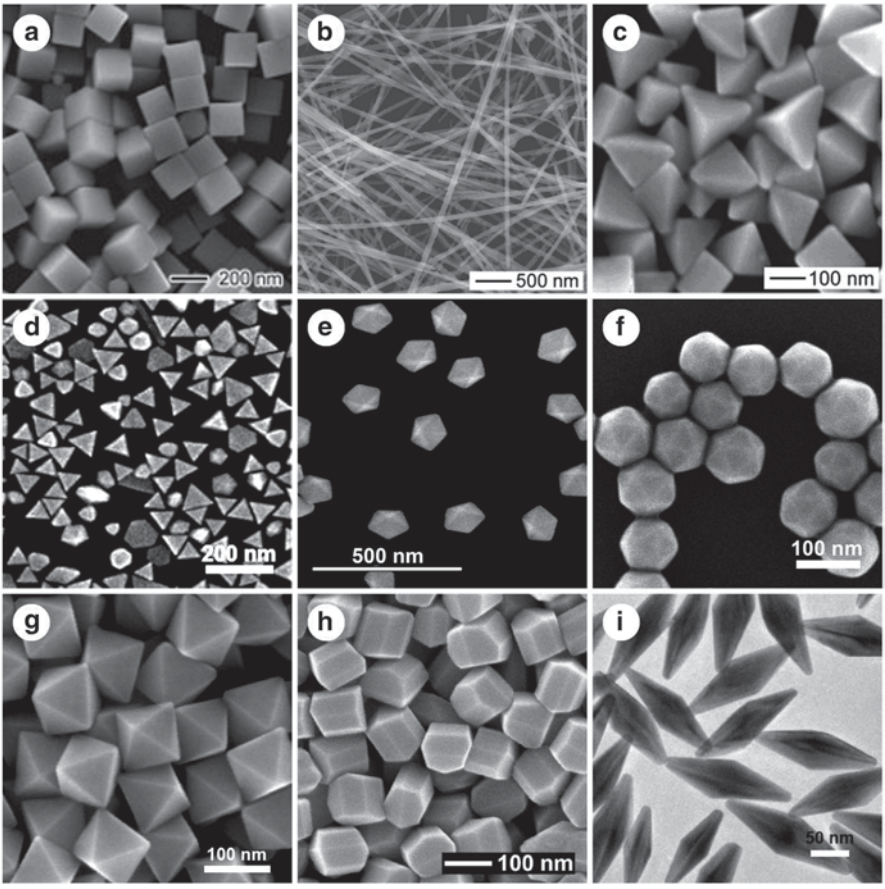

Fig. 1.18 Metallic nanostructures synthesized via polyol processes: **a–c** Ag nanocubes (reproduced with permission from reference [328], Copyright 2005 Wiley-VCH), nanowires (reproduced with permission from reference [312], Copyright 2004 American Chemical Society), and right bipyramids (reproduced with permission from reference [315], Copyright 2006 American Chemical Society), **d–f** Au plate-like, decahedral (reproduced with permission from reference [308], Copyright 2008 American Chemical Society), and icosahedral nanocrystals (reproduced with permission from reference [329], Copyright 2014 American Chemical Society), **g–h** Au octahedra (reproduced with permission from reference [323], Copyright 2008 American Chemical Society), truncated ditetragonal prisms (reproduced with permission from reference [324], Copyright 2011 American Chemical Society), and **i** multiple-twinned bipyramids (reproduced with permission from reference [325], Copyright 2013 The Royal Society of Chemistry)

[315]. A similar strategy is also applied in the synthesis of Pd nanostructure such as Pd nanocubes, nanorods, and nanobars [316–318]. By blocking the oxidative etching of Pd nanostructure with citric acid, multiple-twinned Pd icosahedra were obtained [319]. The Song group showed that by tuning the oxidative etching rate of Au seeds, Au nanocrystals with decahedral, icosahedral, and truncated tetrahedral shapes can be synthesized (Fig. 1.18d–f) [308].

The growth of metallic nanostructures through the polyol process is very sensitive to growth kinetics and inorganic species. For example, the Yang group have shown that the synthesis of Ag nanocrystals with shapes from cubes, to cuboctahedra and octahedra with the assistance of copper(II) chloride [309]. Different shapes can be obtained at different stages of the reaction. By introducing silver nitrate in the growth of Au nanocrystals, Au nanocrystals with continually tunable shapes including octahedra, truncated octahedra, cuboctahedra, cubes, and higher polygons were synthesized, which is attributed to the UPD of silver on the surface of Au nanostructures [242, 320, 321]. By introducing different amounts of silver nitrate, the shapes of platinum nanocrystals could also be tunable across octahedra, cuboctahedra, and cubes [322].

An alternative stabilizing agent for the polyol process is poly(diallyl dimethylammonium chloride) (PDDA). Li et al. developed a PDDA-mediated polyol route to synthesize Au octahedral nanocrystals with high yields and tunable sizes (Fig. 1.18g) [323]. PDDA was believed to selectively stabilize the {111} facets of the Au octahedra. By introducing silver and palladium ions into the growth of Au nanostructures, truncated tetrahexahedra enclosed by {310} and {111} facets, truncated ditetragonal prisms enclosed by {310} facets (Fig. 1.18h), and penta-twinned bipyramids could be obtained [324, 325]. Penta-twinned Au decahedra, Au@Ag core-shell nanorods, and penta-twinned bipyramids (Fig. 1.18i) were also synthesized through Ag(I)-assisted PDDA-mediated polyol processes [325–327].

1.5.3 N,N-Dimethylformamide-Mediated Syntheses

Similar to polyols, N,N-dimethylformamide (DMF) can also be used as a solvent and reducing agent for the synthesis of metallic nanostructures [335]. DMF was first applied as a reaction medium for the synthesis of metallic nanostructures by the Liz-Marzán group in 1999 [336]. In a later work, they showed that Ag nanoplates could be synthesized by using a high silver nitrate concentration and a low PVP concentration (Fig. 1.19a) [330]. Gao et al. synthesized Ag decahedra in DMF with PVP of high molecular weights as a stabilizing agent (Fig. 1.19b) [331]. By increasing the amount of PVP, tetrahedra Ag nanocrystals were obtained. The Xie group reported the synthesis of decahedral Au nanostructures in DMF [337]. By introducing sodium hydroxide, rhombic dodecahedral Au nanocrystals were obtained. Further increasing of the reaction temperature leads to the formation of Au octahedra. Moreover, hexagonal nanosheets were synthesized at a high concentration of Au salts. Subsequent studies have synthesized a few Au nanocrystal enclosed by {110} facets in DMF, including rhombic dodecahedra (Fig. 1.19c), squashed dodecahedra, truncated pentagonal bipyramids (Fig. 1.19d), and Platonic dodecahedra (Fig. 1.19e) [248, 329, 332, 338]. DMF or one of its oxidation products during the reactions is responsible to stabilize the high-energy {110} facets. Xia et al. showed that in an ethylene glycol and DMF mixture, Pt nanowire assemblies composed of ultrathin Pt nanowires were synthesized under solvothermal conditions [122].

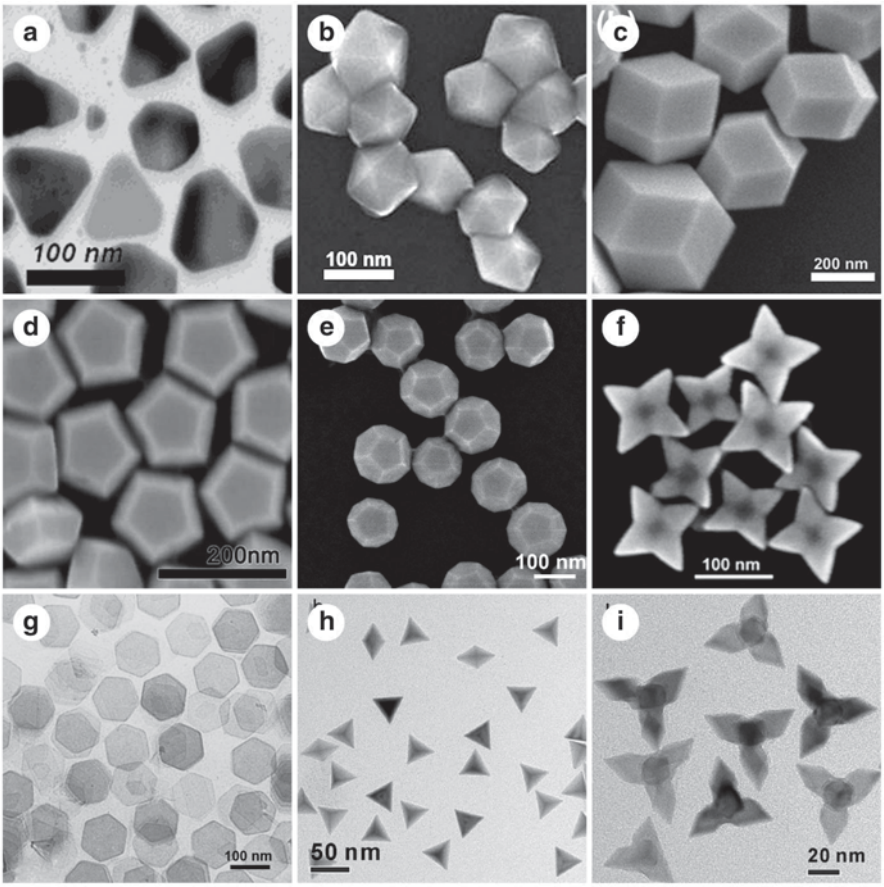

Fig. 1.19 Metallic nanostructures synthesized via N,N-dimethylformamide (DMF)-mediated syntheses: **a** Ag nanoplates (reproduced with permission from reference [330], Copyright 2002 American Chemical Society), **b** Ag decahedral nanocrystals (reproduced with permission from reference [331], Copyright 2006 Elsevier B.V.), **c**–**e** Au rhombic dodecahedra (reproduced with permission from reference [332], Copyright 2009 American Chemical Society), truncated pentagonal bipyramids (reproduced with permission from reference [248], Copyright 2013 The Royal Society of Chemistry), and Platonic dodecahedra (reproduced with permission from reference [329], Copyright 2014 American Chemical Society), **f** concave Pt nanocrystals (reproduced with permission from reference [333], Copyright 2011 American Chemical Society), **g**–**i** Pd nanosheets (reproduced with permission from reference [9], Copyright 2011 Nature Publishing Group), tetrahedra, and tetrapods (reproduced with permission from reference [334], Copyright 2012 American Chemical Society)

A few small molecular adsorbates have been introduced into DMF-mediated reduction to control the morphologies of metallic nanostructures [339]. The Zheng group reported the synthesis of Pt NCs with {411} high-index facets with the addition of short chain amines (Fig. 1.19f). Amines are believed to stabilize the open structures on the {411} surface [333]. By introducing CO, palladium nanosheets with less

than 10-atomic-layer thickness were obtained, due to the growth confinement effect of CO (Fig. 1.19g) [9]. If hydrogen is introduced in addition to CO, single-crystalline Pd tetrapod and tetrahedral nanocrystals enclosed by (111) surfaces can be obtained (Fig. 1.19h–i) [334]. This is due to the fact that CO can stabilize the {111} facets of β-PdH_x nanocrystals, which formed in the presence of H_2 but transformed into pure Pd nanocrystals in air. Cui et al. also reported that CO could be used to confine the growth of Pt−Ni alloy nanoparticles [340].

1.5.4 Oleylamine-Mediated Syntheses

Oleylamine (cis-1-amino-9-octadecene) is a long-chain primary alkylamine broadly used in the synthesis of metallic nanostructures [341]. A variety of metallic nanostructures including Au, Ag, Pt, Pd, and their alloy has been synthesized in the presence of oleylamine. It has several important functions in the synthesis of metallic nanostructure. Oleylamine can simultaneously function as a solvent for the reaction mixture and stabilizing agent for metallic nanostructures. In addition, oleylamine has a boiling point of 364 °C; therefore, it can be used to synthesize metallic nanostructures at high temperatures. Peng et al. used Fourier transform infrared spectroscopy to study the presence of oleylamine on Ag nanoparticles and observed a new peak of Ag–N bonds [342]. Oleylamine-stabilized metallic nanostructures can be easily dispersed in non-polar solvents assisted by the long hydrocarbon chains of the oleylamine molecules. The Sun group has done extensive research on the oleylamine-mediated syntheses of metal nanostructures. For example, monodispersed FePt nanoparticles were synthesized by simultaneous reduction of platinum acetylacetonate and decomposition of iron pentacarbonyl in the presence of oleic acid and oleylamine (Fig. 1.20a) [343]. The composition of the as-synthesized FePt nanoparticles can be controlled by changing the ratio of iron and platinum precursors. Based on oleylamine, they have developed the synthesis protocol for many metallic nanostructures, such Pt, Pd, AgPd, CoPt, NiPt, CuPt, ZnPt, FePtAu alloy nanoparticles, various core-shell structures such as Pd/Au and Pd/Au/FePt core/shell nanoparticles, and Pt-Au heterostructures [344–351].

A few strategies for the shape control of metallic nanostructures have been reported in the oleylamine-mediated syntheses. A typical example is the synthesis of ultrathin Au nanowires in the presence of oleylamine (Fig. 1.20b). Au nanowires can be synthesized in the presence of oleylamine under mild reducing conditions. 1D mesostructures formed between $HAuCl_4$ and oleylamine are believed to act as templates for the growth of Au nanowires [353, 356–360]. Mild reducing conditions can preserve the 1D mesostructure and convert Au salts into metallic nanowires. The Sun group discovered that oleylamine can induce the 1D growth of FePt and CoPt nanostructures (Fig. 1.20c) [354, 361]. Based on this process, 1D FePt, CoPt, FePtCu, FePtNi, and FePtPd nanostructures have been synthesized [354, 361–364]. Ag nanocubes were also synthesized by oleylamine-mediated processes based on oxidative etching process [365–367]. For example, dimethyldistearylammonium

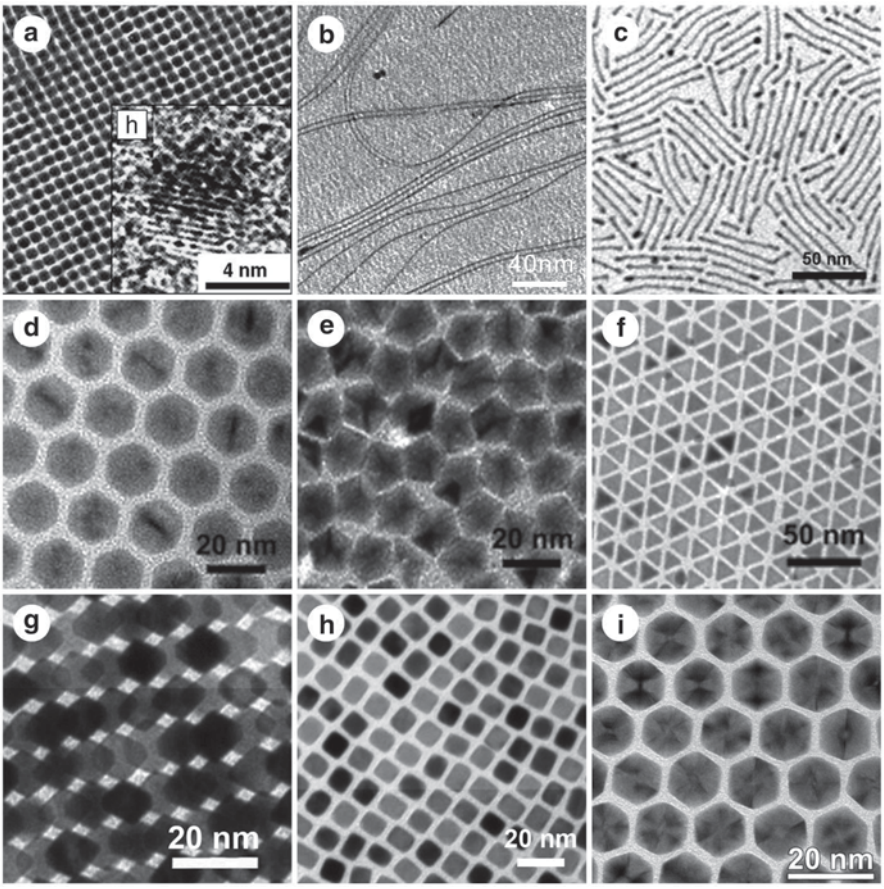

Fig. 1.20 Metallic nanostructures synthesized via oleylamine-mediated synthesis: **a** FePt nanoparticles (reproduced with permission from reference [352], Copyright 2001 Materials Research Society), **b** ultrathin Au nanowires (reproduced with permission from reference [353], Copyright 2008 American Chemical Society), **c** ultrathin FePt nanorods (reproduced with permission from reference [354], Copyright 2007 Wiley-VCH), **d**–**f** Pd icosahedra, decahedra, and triangular plates (reproduced with permission from reference [355], Copyright 2011 Wiley-VCH), **g**–**i** Pt octahedra, cubes (reproduced with permission from reference [218], Copyright 2012 American Chemical Society), and icosahedra (reproduced with permission from reference [221], Copyright 2013 American Chemical Society)

chloride and Fe(III) species were introduced to remove twinned seeds and facilitate the formation of exclusively single-crystalline Ag nanocubes [365, 367]. Pd icosahedral, decahedral, octahedral, tetrahedral, and triangular plate-like Pd NCs were selectively synthesized by introducing formaldehyde and varying the quantities of oleylamine (Fig. 1.20d–f) [355].

Metal carbonyls are an important class of shape-directing agents in oleylamine-mediated syntheses of metal nanostructures. Tungsten hexacarbonyl, iron pentacarbonyl, chromium hexacarbonyl, and dimanganese decacarbonyl have been

explored to control the shapes of metallic nanostructures [218, 368–375]. The Fang group has developed a general strategy to synthesize Pt_3Fe, Pt_3Co, Pt_3Ni nanocubes, and Pt_3Ni nanooctahedra based on tungsten hexacarbonyl-assisted growth in the oleylamine-mediated syntheses [368–370, 374]. The Murray group reported the synthesis of multiple Pt nanostructures with the assistance of dimanganese decacarbonyl (Fig. 1.20g–h) [218]. These structures include truncated cubes, cuboctahedra, spheres, tetrapods, star-shaped octapods, multipods, and hyperbranched structure. Wang and Loukrakpam et al. show that Pt nanocubes could be synthesized in the presence of iron pentacarbonyl and chromium hexacarbonyl, respectively [372, 373]. In these studies, the zero-valence metals from the metal carbonyls were considered to play an essential role for the shape control of Pt nanocubes. Wu et al. proposed that CO from the decomposition of metal carbonyls also plays a major role and promotes the formation of Pt nanocubes [112]. The Murray and Yang groups also directly introduced CO in the oleylamine-mediated syntheses of metallic nanocrystals. A variety of metallic nanostructures have been synthesized through this versatile method, including Pt nanocube, Au nanowires, Pd nanoparticles, icosahedral nanocrystals of Pt (Fig. 1.20i), PtAu, Pt_3Ni, Pt_3Pd, PtPd, nanocubes of Pt_3Ni, PtNi, and $PtNi_3$, octahedral nanocrystals of Pt_3Ni, PtNi, and $PtNi_3$ [7, 221, 376, 377]. This method is named by the Yang group as a gas-reducing agent in liquid solution method. The Tilley group used hydrogen instead of CO as a reducing agent in similar conditions and synthesized monodispersed Pt concave nanocubes and highly branched Pd nanostructures [378–380].

1.5.5 Plasmon-Mediated Syntheses

The interaction of light and plasmonic metallic nanostructures can be employed as a novel tool to synthesize metallic nanostructures with controllable morphologies, especially in the case of Ag nanostructure [152]. In 2001, the Mirkin group first reported that plasmonic photo-excitation of Ag nanostructures could be used to synthesize monodispersed Ag nanoprisms [156]. In their synthesis, spherical Ag nanoparticles were first prepared by the reduction of silver nitrate by sodium borohydride in the presence of trisodium citrate and bis(p-sulfonatophenyl) phenylphosphine dihydrate dipotassium salt (BSPP). Irradiating the Ag nanoparticle solution with visible light results the gradual conversion of spherical nanoparticles into triangular nanoprisms. A plasmon-induced electron transfer mechanism is believed to be responsible for the synthesis of triangular Ag nanoprisms [157, 389–391]. The plasmon excitation of spherical Ag nanoparticles will result in the generation of energetic electron-hole pairs from plasmon decay, which could catalyze the reduction of Ag^+ by citrate, leading to the conversion of spherical nanoparticles into triangular nanoprisms. In the meantime, smaller Ag nanoparticles were oxidized into Ag^+ for the continuous growth of Ag nanoprisms. By using dual-beam illumination, they can improve the synthesis of monodisperse Ag nanoprisms with desired edge lengths in the range of 30–120 nm (Fig. 1.21a) [155]. They also found that edge lengths of the nanoprisms can also be controlled by the pH of the growth solutions [392].

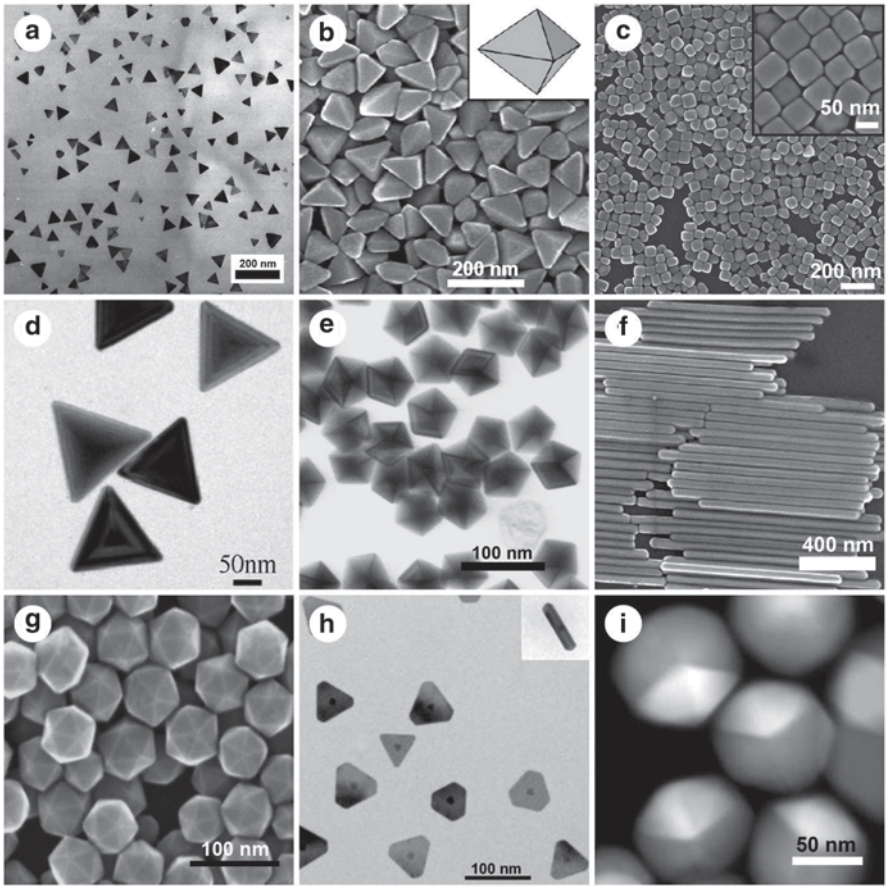

Fig. 1.21 Metallic nanostructures synthesized via plasmon-mediated synthesis: **a** Ag nanoprisms (reproduced with permission from reference [155], Copyright 2003 Nature Publishing Group), **b** Ag right bipyramids (reproduced with permission from reference [381], Copyright 2010 American Chemical Society), **c** twinned Ag nanocubes (reproduced with permission from reference [382], Copyright 2013 Wiley-VCH), **d** Ag tetrahedra (reproduced with permission from reference [383], Copyright 2008 American Chemical Society), **e** Ag decahedra (reproduced with permission from reference [384], Copyright 2008 American Chemical Society), **f** Ag nanorods (reproduced with permission from reference [385], Copyright 2011 American Chemical Society), **g** Ag icosahedra (reproduced with permission from reference [386], Copyright 2014 The Royal Society of Chemistry), **h** Au@Ag core-shell nanoprisms (reproduced with permission from reference [387], Copyright 2007 Wiley-VCH), **i** Au@Ag core-shell icosahedra (reproduced with permission from reference [388], Copyright 2011 Wiley-VCH)

The Ag nanoprisms synthesized through plasmon-mediated syntheses have a multiply planar-twinned structure and are primarily enclosed by {111} facets [152]. By using silver nitrate as a precursor and performing the light-radiation reaction at a higher pH, Ag right triangular bipyramids enclosed by {100} facets were obtained (Fig. 1.21b) [393]. These bipyramids have similar planar-twinned structures. The

selective conversion of these two shapes was realized in a later study [381]. The {100}-faceted right triangular bipyramids are favored at a high pH (>10) and a [BSPP]/[Ag^+] ratio close to 1. Triangular prisms with mostly {111} facets are favored at a lower pH or a higher [BSPP]/[Ag^+] ratio. Ag nanocubes with multiply planar-twinned structures were also synthesized by fine tuning the irradiation wavelength of light during plasmon-mediated syntheses (Fig. 1.21c) [382].

The plasmon-mediated syntheses are capable of producing metallic nanostructures with other crystal structures. For example, with disodium tartrate as a structural-directing agent, tetrahedral Ag nanocrystals enclosed by 4 {111} facets were synthesized with relatively high yields (Fig. 1.21d) [383]. By using arginine as a photochemical promoter, the Kitaev group reported that decahedral Ag nanocrystals with penta-twinned structures were synthesized with a high shape selectivity (Fig. 1.21e) [384]. The Mirkin group reported that at low-energy irradiation wavelengths, Ag penta-twinned nanorods were obtained (Fig. 1.21f) [385]. By using a combination of Cu^{2+} additive, H_2O_2 etchant, and violet light irradiation, the Kitaev group synthesized Ag icosahedral nanoparticles with multiply twinned structures (Fig. 1.21g) [386]. Besides Ag nanostructures, the plasmon-mediated syntheses were also applied in synthesizing Au@Ag core-shell nanostructures by exploring plasmonic Au seeds (Fig. 1.21h–i) [387, 388, 394].

1.5.6 Electrochemical Square-Wave-Potential Methods

Metallic nanostructures with high-energy facets have received considerable attention recently due to their importance in catalytic applications [400, 401]. High-energy facets are usually referred to the {110} and high-index {hkl} facets of metallic nanostructures, which possess a high density of atoms with low coordination numbers and a high density of atomic steps, ledges, and kinks [402]. However, in most common synthetic conditions, the high-energy facets will easily disappear due to their low stability. Electrochemical square-wave-potential (SWP) methods have emerged as a versatile method to synthesize metallic nanostructures with high-energy facets [50, 59]. The Sun pioneered the synthesis of metallic nanostructures with high-energy facets using the electrochemical SWP methods. In 2007, the Sun group reported the synthesis of single-crystalline tetrahexahedral Pt nanocrystals with {730} high-index facets by the electrochemical SWP method [60]. In their report, tetrahexahedral Pt nanocrystals were synthesized by treating electrodeposited ~750 nm Pt nanospheres with SWP of certain lower (E_L) and upper (E_U) potentials in a solution of H_2SO_4 and ascorbic acid. The formation of the high-index {730} facets was attributed to the repetitive adsorption/desorption of oxygen species (OH_{ad} and O_{ad}) generated by SWP processes. At the E_U potential, some of the oxygen species may invade into Pt and squeeze out some Pt atoms. At the E_L, all oxygen species will be desorbed and lead to the formation of Pt surface with open structures. Repeating the SWP process for thousands of times will lead to the formation of Pt nanocrystals with well-defined high-index facets.

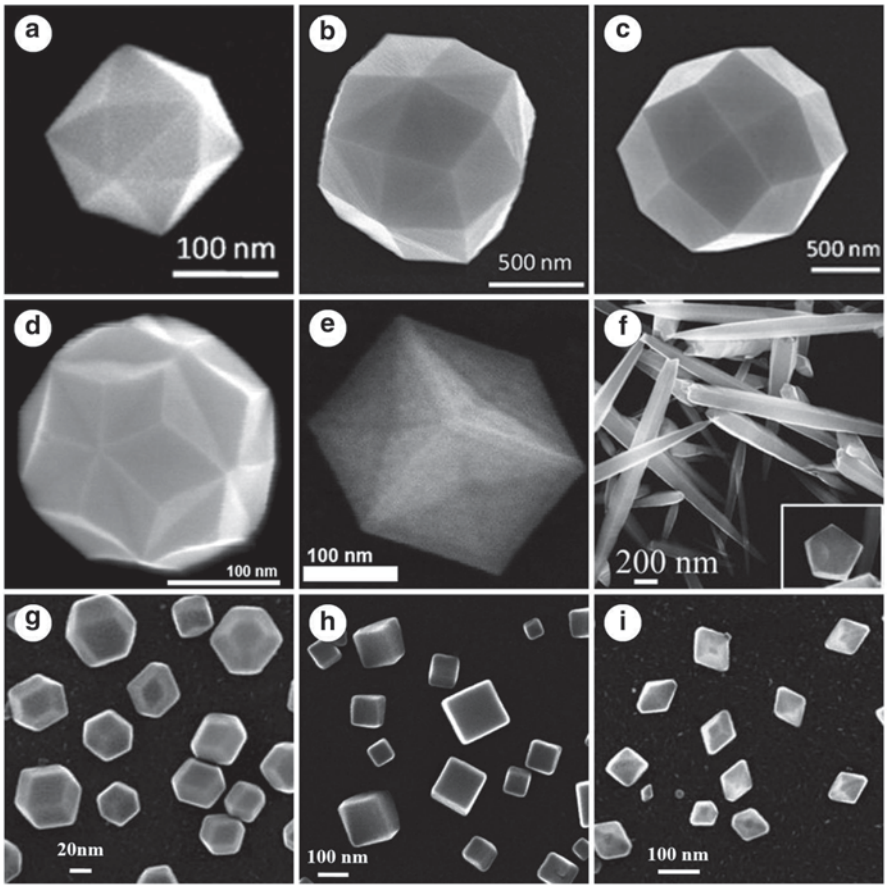

Fig. 1.22 Metallic nanostructures synthesized via electrochemical square-wave-potential (SWP) methods: **a** Pt tetrahexahedra, **b** Pt hexoctahedra, **c** trapezohedra (reproduced with permission from reference [395], Copyright 2013 American Chemical Society), **d** triambic icosahedral Pt nanocrystals (reproduced with permission from reference [396], Copyright 2013 American Chemical Society), **e** concave Pt tetrahexahedra (reproduced with permission from reference [397], Copyright 2011 American Chemical Society), **f** Pd nanorods (reproduced with permission from reference [398], Copyright 2009 The Royal Society of Chemistry), **g–i** Fe rhombic dodecahedra, cubes, and tetragonal bipyramids (reproduced with permission from reference [399], Copyright 2009 American Chemical Society)

The electrochemical SWP methods can be generalized in synthesis various Pt nanocrystals with high-index facets. In a recent report from the Sun group, they described a process that can selectively synthesize tetrahexahedral, hexoctahedral, and trapezohedral Pt nanocrystals, which are enclosed by {hk0}, {hkk}, and {hkl} high-index facets, respectively (Fig. 1.22a–c) [395]. The transition among these different shapes was realized by increasing either the upper or lower potential of the SWP process. Concave hexoctahedral, triambic icosahedral (Fig. 1.22d), concave tetrahexahedral Pt nanocrystals (Fig. 1.22e) were also synthesized through similar electrochemical SWP techniques [50, 396, 397, 403]. The electrochemical SWP

method can also be extended to synthesize other metallic nanostructures, such as tetrahexahedral and trapezohedral Pd nanocrystals, five-fold twinned Pd nanorods (Fig. 1.22f), tetrahexahedral Rh nanocrystals, tetrahexahedral Pd–Pt alloyed nanocrystals, and Fe nanocrystals with different shapes ranging from rhombic dodecahedra to tetragonal bipyramids and cubes (Fig. 1.22g–i) [50, 398, 399, 404–406].

Acknowledgment We thank the Ministry of Education Singapore (Grant# R279-000-391-112) for the financial support of this work.

References

1. C. Burda, X. Chen, R. Narayanan et al., Chem. Rev. **105**, 1025 (2005)
2. R. Vajtai, Springer Handbook of Nanomaterials. (Springer, 2013)
3. K.J. Klabunde, R. Richards, Nanoscale materials in chemistry. (Wiley Online Library, 2001)
4. P. Yang, The chemistry of nanostructured materials. (World Scientific, 2011)
5. R. Nagarajan, T.A. Hatton, Nanoparticles: synthesis, stabilization, passivation, and functionalization. (Oxford University Press, USA, 2008)
6. T.K. Sau, A.L. Rogach, Complex-shaped metal nanoparticles: bottom-up syntheses and applications. (John Wiley & Sons, 2012)
7. Y. Kang, X. Ye, C.B. Murray, Angew. Chem. Int. Ed. **49**, 6156 (2010)
8. X. Ye, L. Jin, H. Caglayan et al., ACS nano **6**, 2804 (2012)
9. X. Huang, S. Tang, X. Mu et al., Nat. Nanotechnol. **6**, 28 (2011)
10. W. Niu, W. Zhang, S. Firdoz et al., Chem. Mater. **26**, 2180 (2014)
11. I. Freestone, N. Meeks, M. Sax et al., Gold Bull. **40**, 270 (2007)
12. D. Barber, I. Freestone, Archaeometry **32**, 33 (1990)
13. S.A. Love, B.J. Marquis, C.L. Haynes, Appl. Spectrosc. **62**, 346A (2008)
14. O. Schalm, V. Van Der Linden, P. Frederickx et al., Spectrochimica Acta B **64**, 812 (2009)
15. S. Padovani, D. Puzzovio, C. Sada et al., Appl. Phys. A **83**, 521 (2006)
16. L. Hunt, Gold Bull. **9**, 134 (1976)
17. B.T. Bell, Rev. Prog. Color. Relat. Top. **9**, 48 (1978)
18. J. Carbert, Gold Bull. **13**, 144 (1980)
19. S. Padovani, I. Borgia, B. Brunetti et al., Appl. Phys. A **79**, 229 (2004)
20. Lycurgus cup, British Museum. http://www.britishmuseum.org/explore/highlights/highlight_objects/pe_mla/t/the_lycurgus_cup.aspx
21. Chartres Cathedral - the Medieval Stained Glass, Whatling Stuart http://www.medievalart.org.uk/index.html
22. P.P. Edwards, J.M. Thomas, Angew. Chem. Int. Ed. **46**, 5480 (2007)
23. R.D. Tweney, Perspect. Sci. **14**, 97 (2006)
24. M. Faraday, Phil. Trans. R. Soc. Lond. 145 (1857)
25. J.M. Thomas, Pure Appl. Chem. **60**, 1517 (1988)
26. V. Sharma, K. Park, M. Srinivasarao, Mat. Sci. Eng. R. **65**, 1 (2009)
27. R. Zsigmondy, Colloids and the ultramicroscope: a manual of colloid chemistry and ultramicroscopy. (J. Wiley & Sons, 1909)
28. R. Zsigmondy, J.F. Norton, E.B. Spear, The chemistry of colloids. (John Wiley & sons, Incorporated, 1917)
29. T. Svedberg, The formation of colloids. (D. Van Nostrand, 1921)
30. T. Svedberg, K.O. Pedersen, The Ultracentrifuge. (1940)
31. J. Turkevich, J. Hillier, Anal. Chem. **21**, 475 (1949)
32. D. Beischer, And Krause, F. , Naturwissenschaften **25**, 825 (1937)
33. P. Cooperástevenson, Discuss. Faraday Soc. **11**, 55 (1951)

34. G. Frens, Nature **241**, 20 (1973)
35. Z.L. Wang, Characterization of nanophase materials. (Wiley Online Library, 2000)
36. Y. Zhu, R. Jin, Y. Sun, Catalysts **1**, 3 (2011)
37. K. An, G.A. Somorjai, ChemCatChem **4**, 1512 (2012)
38. P. Mulvaney, MRS Bull. **26**, 1009 (2001)
39. L.N. Lewis, Chem. Rev. **93**, 2693 (1993)
40. E.C. Dreaden, A.M. Alkilany, X. Huang et al., Chem. Soc. Rev. **41**, 2740 (2012)
41. K.A. Willets, R.P. Van Duyne, Annu. Rev. Phys. Chem. **58**, 267 (2007)
42. H. Chen, L. Shao, Q. Li et al., Chem. Soc. Rev. **42**, 2679 (2013)
43. J. Zhao, X.Y. Zhang, C.R. Yonzon et al., Nanomedicine **1**, 219 (2006)
44. H.A. Atwater, A. Polman, Nat. Mater. **9**, 205 (2010)
45. A.J. Haes, R.P. Van Duyne, Anal. Bioanal. Chem. **379**, 920 (2004)
46. K. Ueno, H. Misawa, J. Photochem. Photobiol., C **15**, 31 (2013)
47. J.L. West, N.J. Halas, Annu. Rev. Biomed. Eng. **5**, 285 (2003)
48. S.E. Skrabalak, L. Au, X. Li et al., Nat. Protoc. **2**, 2182 (2007)
49. B. Sepúlveda, P.C. Angelomé, L.M. Lechuga et al., Nano Today **4**, 244 (2009)
50. N. Tian, Z.-Y. Zhou, S.-G. Sun, J. Phys. Chem. C **112**, 19801 (2008)
51. F. Zaera, ChemSusChem **6**, 1797 (2013)
52. B. Roldan Cuenya, Acc. Chem. Res. **46**, 1682 (2012)
53. S. Cheong, J.D. Watt, R.D. Tilley, Nanoscale **2**, 2045 (2010)
54. J. Wu, P. Li, Y.-T.F. Pan et al., Chem. Soc. Rev. **41**, 8066 (2012)
55. Y. Li, G.A. Somorjai, Nano Lett. **10**, 2289 (2010)
56. M. Haruta, Nature **437**, 1098 (2005)
57. M. Haruta, N. Yamada, T. Kobayashi et al., J. Catal. **115**, 301 (1989)
58. Y. Xiong, B.J. Wiley, Y. Xia, Angew. Chem. Int. Ed. **46**, 7157 (2007)
59. Z.-Y. Zhou, N. Tian, Z.-Z. Huang et al., Faraday Discuss. **140**, 81 (2009)
60. N. Tian, Z.-Y. Zhou, S.-G. Sun et al., science **316**, 732 (2007)
61. K.M. Bratlie, H. Lee, K. Komvopoulos et al., Nano Lett. **7**, 3097 (2007)
62. Y.-W. Jun, J.-W. Seo, J. Cheon, Acc. Chem. Res. **41**, 179 (2008)
63. S.P. Gubin, Magnetic nanoparticles. (John Wiley & Sons, 2009)
64. A.P. Guimarães, Principles of nanomagnetism. (Springer, 2009)
65. Y.-W. Jun, J.-S. Choi, J. Cheon, Chem . Commun. 1203 (2007)
66. J.I. Park, N.J. Kang, Y.W. Jun et al., ChemPhysChem **3**, 543 (2002)
67. J.-R. Choi, S.J. Oh, H. Ju et al., Nano Lett. **5**, 2179 (2005)
68. J.-I. Park, M.G. Kim, Y.-W. Jun et al., J. Am. Chem. Soc. **126**, 9072 (2004)
69. J.-I. Park, J. Cheon, J. Am. Chem. Soc. **123**, 5743 (2001)
70. M.A. El-Sayed, Acc. Chem. Res. **34**, 257 (2001)
71. D. Wang, Y. Li, Adv. Mater. **23**, 1044 (2011)
72. Y. Xia, Y. Xiong, B. Lim et al., Angew. Chem. Int. Ed. **48**, 60 (2009)
73. A.A. Ashkarran, J. Cluster Sci. **22**, 233 (2011)
74. N.G. Semaltianos, Crit . Rev. Solid State Mater. Sci. **35**, 105 (2010)
75. F.B. De Mongeot, U. Valbusa, J. Phys.. Condens. Matter. **21**, (2009)
76. A. Botman, J.J.L. Mulders, C.W. Hagen, Nanotechnology **20**, (2009)
77. Z.R. Dai, Z.W. Pan, Z.L. Wang, Adv. Funct. Mater. **13**, 9 (2003)
78. M. Altissimo, Biomicrofluidics **4**, 026503 (2010)
79. S. Gao, K. Ueno, H. Misawa, Acc. Chem. Res. **44**, 251 (2011)
80. J. Henzie, J. Lee, M.H. Lee et al., Annu. Rev. Phys. Chem. **60**, 147 (2009)
81. X. Ye, L. Qi, Nano Today **6**, 608 (2011)
82. C.L. Haynes, R.P. Van Duyne, J. Phys. Chem. B **105**, 5599 (2001)
83. M. Seipenbusch, A. Binder, J. Phys. Chem. C **113**, 20606 (2009)
84. J. Lu, J.W. Elam, P.C. Stair, Acc. Chem. Res. **46**, 1806 (2013)
85. J. Lu, K.-B. Low, Y. Lei et al., Nat. Commun. **5**, 3264 (2014)
86. M. Knez, K. Nielsch, L. Niinistö, Adv. Mater. **19**, 3425 (2007)
87. S.M. George, Chem. Rev. **110**, 111 (2009)

88. G.H. Chan, J. Zhao, E.M. Hicks et al., Nano Lett. **7**, 1947 (2007)
89. J. Henzie, E.-S. Kwak, T.W. Odom, Nano Lett. **5**, 1199 (2005)
90. C.N.J. Wagner, J. Non-Cryst. Solids **150**, 1 (1992)
91. S. Orimo, H. Fujii, Intermetallics **6**, 185 (1998)
92. A.R. Tao, S. Habas, P. Yang, Small **4**, 310 (2008)
93. W.X. Niu, G.B. Xu, Nano Today **6**, 265 (2011)
94. D. Wang, T. Xie, Y. Li, Nano Research **2**, 30 (2009)
95. Q.A. Yuan, X. Wang, Nanoscale **2**, 2328 (2010)
96. M.C. Daniel, D. Astruc, Chem. Rev. **104**, 293 (2004)
97. J.Y. Xiao, L.M. Qi, Nanoscale **3**, 1383 (2011)
98. T.H. Ha, H.-J. Koo, B.H. Chung, J. Phys. Chem. C **111**, 1123 (2006)
99. S.E. Lohse, N.D. Burrows, L. Scarabelli et al., Chem. Mater. **26**, 34 (2013)
100. X. Lu, T.T. Tran, W. Zhang, Chem. Eng. Process. Tech. **1**, 1009 (2013)
101. J.U. Kim, S.H. Cha, K. Shin et al., Adv. Mater. **16**, 459 (2004)
102. C.-Y. Chiu, Y. Li, L. Ruan et al., Nature chemistry **3**, 393 (2011)
103. L. Ruan, C.-Y. Chiu, Y. Li et al., Nano Lett. **11**, 3040 (2011)
104. J. Xie, J.Y. Lee, D.I. Wang et al., ACS nano **1**, 429 (2007)
105. J. Xie, J.Y. Lee, D.I. Wang et al., Small **3**, 672 (2007)
106. C.-Y. Chiu, L. Ruan, Y. Huang, Chem. Soc. Rev. **42**, 2512 (2013)
107. J.R. Thomas, J. Appl. Phys. **37**, 2914 (1966)
108. D. Decaro, T. Ould-Ely, A. Mari et al., Chem. Mater. **8**, 1987 (1996)
109. V.F. Puntes, K.M. Krishnan, A.P. Alivisatos, Science **291**, 2115 (2001)
110. S.J. Park, S. Kim, S. Lee et al., J. Am. Chem. Soc. **122**, 8581 (2000)
111. T.O. Ely, C. Amiens, B. Chaudret et al., Chem. Mater. **11**, 526 (1999)
112. B. Wu, N. Zheng, G. Fu, Chem. Commun. **47**, 1039 (2011)
113. M. Grzelczak, J. Pérez-Juste, P. Mulvaney et al., Chem. Soc. Rev. **37**, 1783 (2008)
114. Y. Sun, Chem. Soc. Rev. **42**, 2497 (2013)
115. C.D. Donega, P. Liljeroth, D. Vanmaekelbergh, Small **1**, 1152 (2005)
116. S.G. Kwon, T. Hyeon, Small **7**, 2685 (2011)
117. C.J. Murphy, T.K. Sau, A.M. Gole et al., J. Phys. Chem. B **109**, 13857 (2005)
118. W. Niu, L. Zhang, G. Xu, Nanoscale **5**, 3172 (2013)
119. W. Niu, L. Zhang, G. Xu, Sci. China Chem. **55**, 2311 (2012)
120. C.J. Murphy, A.M. Gole, S.E. Hunyadi et al., Inorg. Chem. **45**, 7544 (2006)
121. X. Huang, N. Zheng, J. Am. Chem. Soc. **131**, 4602 (2009)
122. B.Y. Xia, H.B. Wu, Y. Yan et al., J. Am. Chem. Soc. **135**, 9480 (2013)
123. Y. Yu, Y. Zhao, T. Huang et al., Pure Appl. Chem. **81**, (2009)
124. F. Kim, J.H. Song, P. Yang, J. Am. Chem. Soc. **124**, 14316 (2002)
125. S.-S. Chang, C.-W. Shih, C.-D. Chen et al., Langmuir **15**, 701 (1998)
126. J. Zhang, J. Du, B. Han et al., Angew. Chem. **118**, 1134 (2006)
127. W.T. Yao, S.H. Yu, Int. J. Nanotechnol. **4**, 129 (2007)
128. Y.J. Li, H. Zhu, C. Hon et al., Prog. Chem. **25**, 276 (2013)
129. W.D. Shi, S.Y. Song, H.J. Zhang, Chem. Soc. Rev. **42**, 5714 (2013)
130. S. Feng, R. Xu, Acc. Chem. Res. **34**, 239 (2001)
131. B.A. Xu, X. Wang, Dalton Trans. **41**, 4719 (2012)
132. D. Yu, V.W.-W. Yam, J. Am. Chem. Soc. **126**, 13200 (2004)
133. D. Yu, V.W.-W. Yam, J. Phys. Chem. B **109**, 5497 (2005)
134. X. Sun, Y. Li, Adv. Mater. **17**, 2626 (2005)
135. Y. Jia, Y. Jiang, J. Zhang et al., J. Am. Chem. Soc. **136**, 3748 (2014)
136. F. Saleem, Z. Zhang, B. Xu et al., J. Am. Chem. Soc. **135**, 18304 (2013)
137. H. Duan, N. Yan, R. Yu et al., Nat. Commun. **5**, 3093 (2014)
138. X. Huang, S. Tang, H. Zhang et al., J. Am. Chem. Soc. **131**, 13916 (2009)
139. Z.-C. Zhang, J.-F. Hui, Z.-C. Liu et al., Langmuir **28**, 14845 (2012)
140. M. Chen, B.H. Wu, J. Yang et al., Adv. Mater. **24**, 862 (2012)
141. M. Tsuji, M. Hashimoto, Y. Nishizawa et al., Chem. Eur. J **11**, 440 (2005)

142. M. Baghbanzadeh, L. Carbone, P.D. Cozzoli et al., Angew. Chem. Int. Ed. **50**, 11312 (2011)
143. T. Yamamoto, Y. Wada, T. Sakata et al., Chem. Lett. **33**, 158 (2004)
144. N. Elander, J.R. Jones, S.-Y. Lu et al., Chem. Soc. Rev. **29**, 239 (2000)
145. W. Tu, H. Liu, J. Mater. Chem. **10**, 2207 (2000)
146. Y. Yu, Y. Zhao, T. Huang et al., Mater. Res. Bull. **45**, 159 (2010)
147. X. Tong, Y. Zhao, T. Huang et al., Appl. Surf. Sci. **255**, 9463 (2009)
148. A. Abedini, A.R. Daud, M.a.A. Hamid et al. , Nanoscale Res. Lett. **8**, 1 (2013)
149. J. Marignier, J. Belloni, M. Delcourt et al., (1985)
150. J. Belloni, Catal. Today **113**, 141 (2006)
151. Y. Niidome, K. Nishioka, H. Kawasaki et al., Chem. Commun. 2376 (2003)
152. M.R. Langille, M.L. Personick, C.A. Mirkin, Angew. Chem. Int. Ed. **52**, 13910 (2013)
153. Y. Sun, Y. Xia, Adv. Mater. **15**, 695 (2003)
154. Y. Sun, B. Mayers, Y. Xia, Nano Lett. **3**, 675 (2003)
155. R.C. Jin, Y.C. Cao, E.C. Hao et al., Nature **425**, 487 (2003)
156. R.C. Jin, Y.W. Cao, C.A. Mirkin et al., Science **294**, 1901 (2001)
157. X. Wu, P.L. Redmond, H. Liu et al., J. Am. Chem. Soc. **130**, 9500 (2008)
158. M.T. Reetz, W. Helbig, S.A. Quaiser et al., Science **267**, 367 (1995)
159. M.T. Reetz, W. Helbig, J. Am. Chem. Soc. **116**, 7401 (1994)
160. Y.-Y. Yu, S.-S. Chang, C.-L. Lee et al., J. Phys. Chem. B **101**, 6661 (1997)
161. H. Xu, B.W. Zeiger, K.S. Suslick, Chem. Soc. Rev. **42**, 2555 (2013)
162. Y.-J. Zhu, F. Chen, Chem. Rev. **114**, 6462 (2014)
163. E. Carbó-Argibay, B. Rodríguez-González, J. Pacifico et al., Angew. Chem. **119**, 9141 (2007)
164. A. Sánchez-Iglesias, I. Pastoriza-Santos, J. Pérez-Juste et al., Adv. Mater. **18**, 2529 (2006)
165. L.-P. Jiang, S. Xu, J.-M. Zhu et al., Inorg. Chem. **43**, 5877 (2004)
166. K. Okitsu, K. Sharyo, R. Nishimura, Langmuir **25**, 7786 (2009)
167. H. Xu, K.S. Suslick, ACS nano **4**, 3209 (2010)
168. H. Liu, X. Zhang, X. Wu et al., Chem. Commun. **47**, 4237 (2011)
169. K.S. Suslick, Y. Didenko, M.M. Fang et al., Philos. Trans. A Math. Phys. Eng. Sci. **357**, 335 (1999)
170. K.S. Suslick, S.-B. Choe, A.A. Cichowlas et al., Nature **353**, 414 (1991)
171. K.S. Suslick, G.J. Price, Annu. Rev. Mater. Sci. **29**, 295 (1999)
172. R.A. Caruso, M. Ashokkumar, F. Grieser, Langmuir **18**, 7831 (2002)
173. L. Qi, Encyclopedia of Surface and Colloid Science. Second Edition. New York: Taylor & Francis 6183 (2006)
174. V.T. Liveri, Reversed micelles as nanometer-size solvent media. (Marcel Dekker: New York, 2002)
175. I. Lisiecki, J. Phys. Chem. B **109**, 12231 (2005)
176. J. Klier, C.J. Tucker, T.H. Kalantar et al., Adv. Mater. **12**, 1751 (2000)
177. J. Eastoe, M.J. Hollamby, L. Hudson, Adv. Colloid Interface Sci. **128**, 5 (2006)
178. M. Pileni, J. Phys. Chem. **97**, 6961 (1993)
179. M.P. Pileni, Langmuir **13**, 3266 (1997)
180. X. Wang, Q. Peng, Y. Li, Acc. Chem. Res. **40**, 635 (2007)
181. L.M. Liz-Marzan, Chem. Commun. **49**, 16 (2013)
182. Q. Yao, Y. Yu, X. Yuan et al., Small **9**, 2696 (2013)
183. M. Brust, J. Fink, D. Bethell et al., J. Chem. Soc., Chem. Commun. 1655 (1995)
184. M. Brust, M. Walker, D. Bethell et al., J. Chem. Soc., Chem. Commun. 801 (1994)
185. X. Wang, J. Zhuang, Q. Peng et al., Nature **437**, 121 (2005)
186. N.R. Jana, Small **1**, 875 (2005)
187. Y.J. Xiong, H.G. Cai, B.J. Wiley et al., J. Am. Chem. Soc. **129**, 3665 (2007)
188. B.J. Wiley, Y. Chen, J.M. Mclellan et al., Nano Lett. **7**, 1032 (2007)
189. Y. Sun, Y. Xia, Adv. Mater. **14**, 833 (2002)
190. B.J. Wiley, Z. Wang, J. Wei et al., Nano Lett. **6**, 2273 (2006)
191. X. Liu, N. Wu, B.H. Wunsch et al., Small **2**, 1046 (2006)

192. M.R. Jones, K.D. Osberg, R.J. Macfarlane et al., Chem. Rev. **111**, 3736 (2011)
193. Y. Liu, J. Goebl, Y. Yin, Chem. Soc. Rev. **42**, 2610 (2013)
194. H. Wang, G.P. Goodrich, F. Tam et al., J. Phys. Chem. B **109**, 11083 (2005)
195. C. Gao, Q. Zhang, Z. Lu et al., J. Am. Chem. Soc. **133**, 19706 (2011)
196. H. Wang, H.Y. Jeong, M. Imura et al., J. Am. Chem. Soc. **133**, 14526 (2011)
197. M.J. Banholzer, L. Qin, J.E. Millstone et al., Nat. Protoc. **4**, 838 (2009)
198. L. Polavarapu, L.M. Liz-Marzan, Nanoscale **5**, 4355 (2013)
199. H.W. Liang, S. Liu, J.Y. Gong et al., Adv. Mater. **21**, 1850 (2009)
200. R.M. Crooks, M. Zhao, L. Sun et al., Acc. Chem. Res. **34**, 181 (2001)
201. H.L. Qin, D. Wang, Z.L. Huang et al., J. Am. Chem. Soc. **135**, 12544 (2013)
202. J. Niu, D. Wang, H. Qin et al., Nat. Commun. **5**, 3313 (2014)
203. H. Wang, D.W. Brandl, P. Nordlander et al., Acc. Chem. Res. **40**, 53 (2007)
204. C. Loo, A. Lin, L. Hirsch et al., Technol. Cancer. Res. Treat. **3**, 33 (2004)
205. S.J. Oldenburg, R.D. Averitt, S.L. Westcott et al., Chem. Phys. Lett. **288**, 243 (1998)
206. P. Karthika, H. Ataee-Esfahani, H.J. Wang et al., Chem. Asian J. **8**, 902 (2013)
207. H.J. Wang, M. Imura, Y. Nemoto et al., Chem. Asian J. **7**, 802 (2012)
208. C. Martin, Science **266**, 1961 (1994)
209. Y.Z. Piao, H. Kim, J. nanosci. nanotechnol. **9**, 2215 (2009)
210. M.E. Toimil-Molares, Beilstein J. Nanotechnol. **3**, 860 (2012)
211. T.R. Kline, M. Tian, J. Wang et al., Inorg. Chem. **45**, 7555 (2006)
212. L.D. Qin, S. Park, L. Huang et al., Science **309**, 113 (2005)
213. A.B. Braunschweig, A.L. Schmucker, W.D. Wei et al., Chem. Phys. Lett. **486**, 89 (2010)
214. S.E. Skrabalak, J. Chen, Y. Sun et al., Acc. Chem. Res. **41**, 1587 (2008)
215. B. Mayers, X. Jiang, D. Sunderland et al., J. Am. Chem. Soc. **125**, 13364 (2003)
216. Y. Qin, R. Che, C. Liang et al., J. Mater. Chem. **21**, 3960 (2011)
217. J. Fang, S. Lebedkin, S. Yang et al., Chem. Commun. **47**, 5157 (2011)
218. Y. Kang, J.B. Pyo, X. Ye et al., ACS nano **7**, 645 (2012)
219. X. Xia, S.-I. Choi, J.A. Herron et al., J. Am. Chem. Soc. **135**, 15706 (2013)
220. J.L. Elechiguerra, J. Reyes-Gasga, M.J. Yacaman, J. Mater. Chem. **16**, 3906 (2006)
221. W. Zhou, J. Wu, H. Yang, Nano Lett. **13**, 2870 (2013)
222. D.B. Williams, C.B. Carter, Micron **28**, 75 (1997)
223. P.W. Hawkes, Advances in imaging and electron physics. (Academic Press, 2003)
224. B. Schmidt, K. Wetzig, Ion beams in materials processing and analysis. (Springer, 2012)
225. J.J. Bozzola, L.D. Russell, Electron microscopy: principles and techniques for biologists. (Jones & Bartlett Learning, 1999)
226. S.C. Singh, H. Zeng, C. Guo et al., Nanomaterials: processing and characterization with lasers. (John Wiley & Sons, 2012)
227. K. Ramesh, Nanomaterials : Mechanics and Mechanisms. (Dordrecht: Springer, 2009)
228. L. Reimer, Meas. Sci. Technol. **11**, 1826 (2000)
229. C. Zweben, JOM **50**, 47 (1998)
230. S. Sharma, Atomic and Nuclear Physics. (Pearson Education India, 2008)
231. R. Jalilian, Pulse Laser Assisted Growth of Nanowires and Nano-heterojunctions and Their Properties. (ProQuest, 2008)
232. J. Henzie, M. Grünwald, A. Widmer-Cooper et al., Nat. Mater. **11**, 131 (2012)
233. X. Ye, Y. Gao, J. Chen et al., Nano Lett. **13**, 2163 (2013)
234. G. Haugstad, Atomic force microscopy : understanding basic modes and advanced applications. (John Wiley & Sons, 2012)
235. K.S. Breuer, Microscale diagnostic techniques. (Springer, 2005)
236. R.W. Kelsall, I.W. Hamley, M. Geoghegan, Nanoscale science and technology. (Wiley Online Library, 2005)
237. G. Binnig, C.F. Quate, C. Gerber, Phys. Rev. Lett. **56**, 930 (1986)
238. X.C. Tong, Advanced materials for thermal management of electronic packaging. (Springer, 2011)

239. Y. Waseda, E. Matsubara, K. Shinoda, X-ray diffraction crystallography: introduction, examples and solved problems. (Springer, 2011)
240. M. Rai, N. Duran, G. Southam, Metal nanoparticles in microbiology. (Springer, 2011)
241. R. Saravanan, M.P. Rani, Metal and Alloy Bonding: An Experimental Analysis. (Springer, 2012)
242. D. Seo, J.C. Park, H. Song, J. Am. Chem. Soc. **128**, 14863 (2006)
243. X. Zou, S. Hovmöller, P. Oleynikov, Electron Crystallography : electron microscopy and electron diffraction. (Oxford University Press, 2011)
244. P.J. Goodhew, J. Humphreys, R. Beanland, Electron microscopy and analysis. (CRC Press, 2000)
245. D.L. Schodek, P. Ferreira, M.F. Ashby, Nanomaterials, nanotechnologies and design : an introduction for engineers and architects. (Butterworth-Heinemann, 2009)
246. P.D. Brown, Transmission Electron Microscopy-A Textbook for Materials Science. (Cambridge Univ Press, 1999)
247. W. Niu, L. Zhang, G. Xu, Acs Nano **4**, 1987 (2010)
248. T. Liu, P. Jiang, Q. You et al., CrystEngComm **15**, 2350 (2013)
249. S. Hofmann, Auger-and X-ray Photoelectron Spectroscopy in Materials Science: A User-oriented Guide. (Springer, 2012)
250. K. Nogi, M. Hosokawa, M. Naito et al., Nanoparticle technology handbook. (Elsevier, 2012)
251. J.P. Davim, Surface integrity in machining. (Springer, 2010)
252. A. Dimoulas, E. Gusev, P.C. Mcintyre et al., Advanced gate stacks for high-mobility semiconductors. (Springer, 2008)
253. M.L. Personick, M.R. Langille, J. Zhang et al., Nano Lett. **11**, 3394 (2011)
254. D. Bell, A. Garratt-Reed, Energy dispersive X-ray analysis in the electron microscope. (Garland Science, 2003)
255. C.R. Brundle, C.A. Evans, S. Wilson, Encyclopedia of materials characterization: surfaces, interfaces, thin films. (Gulf Professional Publishing, 1992)
256. G. Agostini, C. Lamberti, Characterization of semiconductor heterostructures and nanostructures. (Elsevier, 2011)
257. W. Zhang, H.Y.J. Goh, S. Firdoz et al., Chem. Eur. J **19**, 12732 (2013)
258. G.L. Moore, Introduction to inductively coupled plasma atomic emission spectrometry. (Elsevier, 2012)
259. H.E. Taylor, Inductively coupled plasma-mass spectrometry : practices and techniques. (Academic Press, 2001)
260. J.R. Dean, Practical inductively coupled plasma spectroscopy. (John Wiley & Sons, 2005)
261. M.J. Brisson, A.A. Ekechukwu, Beryllium : environmental analysis and monitoring. (Royal Society of Chemistry, 2009)
262. P. Szefer, J.O. Nriagu, Mineral components in foods. (CRC Press, 2006)
263. R.A. Scott, C.M. Lukehart, Applications of physical methods to inorganic and bioinorganic chemistry. (John Wiley & Sons, 2013)
264. H.-C. Peng, S. Xie, J. Park et al., J. Am. Chem. Soc. **135**, 3780 (2013)
265. S.E. Lohse, C.J. Murphy, Chem. Mater. **25**, 1250 (2013)
266. K.R. Brown, L.A. Lyon, A.P. Fox et al., Chem. Mater. **12**, 314 (1999)
267. K.R. Brown, M.J. Natan, Langmuir **14**, 726 (1998)
268. K.R. Brown, D.G. Walter, M.J. Natan, Chem. Mater. **12**, 306 (1999)
269. N.R. Jana, L. Gearheart, C.J. Murphy, Chem . Commun. 617 (2001)
270. N.R. Jana, L. Gearheart, C.J. Murphy, J. Phys. Chem. B **105**, 4065 (2001)
271. C.J. Johnson, E. Dujardin, S.A. Davis et al., J. Mater. Chem. **12**, 1765 (2002)
272. A. Gole, C.J. Murphy, Chem. Mater. **16**, 3633 (2004)
273. N.R. Jana, Chem. Commun. 1950 (2003)
274. B. Nikoobakht, M.A. El-Sayed, Chem. Mater. **15**, 1957 (2003)
275. T.K. Sau, C.J. Murphy, Langmuir **20**, 6414 (2004)
276. H.-Y. Wu, H.-C. Chu, T.-J. Kuo et al., Chem. Mater. **17**, 6447 (2005)

277. H.-Y. Wu, W.-L. Huang, M.H. Huang, Cryst. Growth Des. **7**, 831 (2007)
278. L. Gou, C.J. Murphy, Chem. Mater. **17**, 3668 (2005)
279. M. Liu, P. Guyot-Sionnest, J. Phys. Chem. B **109**, 22192 (2005)
280. X. Kou, S. Zhang, C.-K. Tsung et al., J. Phys. Chem. B **110**, 16377 (2006)
281. X. Kou, S. Zhang, C.K. Tsung et al., Chem. Eur. J **13**, 2929 (2007)
282. X. Ye, C. Zheng, J. Chen et al., Nano Lett. **13**, 765 (2013)
283. T.K. Sau, C.J. Murphy, J. Am. Chem. Soc. **126**, 8648 (2004)
284. W. Niu, S. Zheng, D. Wang et al., J. Am. Chem. Soc. **131**, 697 (2008)
285. H.-L. Wu, C.-H. Kuo, M.H. Huang, Langmuir **26**, 12307 (2010)
286. M. Eguchi, D. Mitsui, H.-L. Wu et al., Langmuir **28**, 9021 (2012)
287. Y. Yu, Q. Zhang, X. Lu et al., J. Phys. Chem. C **114**, 11119 (2010)
288. M.R. Langille, M.L. Personick, J. Zhang et al., J. Am. Chem. Soc. **134**, 14542 (2012)
289. M.L. Personick, C.A. Mirkin, J. Am. Chem. Soc. **135**, 18238 (2013)
290. T. Ming, W. Feng, Q. Tang et al., J. Am. Chem. Soc. **131**, 16350 (2009)
291. J. Li, L. Wang, L. Liu et al., Chem. Commun. **46**, 5109 (2010)
292. M.L. Personick, M.R. Langille, J. Zhang et al., J. Am. Chem. Soc. **133**, 6170 (2011)
293. F. Lu, Y. Zhang, L. Zhang et al., J. Am. Chem. Soc. **133**, 18074 (2011)
294. M.L. Personick, M.R. Langille, J. Wu et al., J. Am. Chem. Soc. **135**, 3800 (2013)
295. J. Zhang, M.R. Langille, M.L. Personick et al., J. Am. Chem. Soc. **132**, 14012 (2010)
296. Y. Yu, Q. Zhang, J. Xie et al., Nat. Commun. **4**, 1454 (2013)
297. W. Niu, Z.-Y. Li, L. Shi et al., Cryst. Growth Des. **8**, 4440 (2008)
298. B.T. Sneed, C.-H. Kuo, C.N. Brodsky et al., J. Am. Chem. Soc. **134**, 18417 (2012)
299. F.-R. Fan, D.-Y. Liu, Y.-F. Wu et al., J. Am. Chem. Soc. **130**, 6949 (2008)
300. Y.-C. Tsao, S. Rej, C.-Y. Chiu et al., J. Am. Chem. Soc. (2013)
301. C.-W. Yang, K. Chanda, P.-H. Lin et al., J. Am. Chem. Soc. **133**, 19993 (2011)
302. C.-L. Lu, K.S. Prasad, H.-L. Wu et al., J. Am. Chem. Soc. **132**, 14546 (2010)
303. Y. Yu, Q. Zhang, B. Liu et al., J. Am. Chem. Soc. **132**, 18258 (2010)
304. S.E. Habas, H. Lee, V. Radmilovic et al., Nat. Mater. **6**, 692 (2007)
305. Y.-H. Chen, H.-H. Hung, M.H. Huang, J. Am. Chem. Soc. **131**, 9114 (2009)
306. P.J. Chung, L.M. Lyu, M.H. Huang, Chem. Eur. J **17**, 9746 (2011)
307. B. Wiley, Y. Sun, B. Mayers et al., Chem. Eur. J **11**, 454 (2005)
308. D. Seo, C.I. Yoo, I.S. Chung et al., J. Phys. Chem. C **112**, 2469 (2008)
309. A. Tao, P. Sinsermsuksakul, P. Yang, Angew. Chem. Int. Ed. **45**, 4597 (2006)
310. Y. Sun, Y. Xia, Science **298**, 2176 (2002)
311. Y. Zheng, J. Zeng, A. Ruditskiy et al., Chem. Mater. (2013)
312. B. Wiley, T. Herricks, Y. Sun et al., Nano Lett. **4**, 1733 (2004)
313. S.H. Im, Y.T. Lee, B. Wiley et al., Angew. Chem. Int. Ed. **44**, 2154 (2005)
314. Y. Sun, B. Gates, B. Mayers et al., Nano Lett. **2**, 165 (2002)
315. B.J. Wiley, Y. Xiong, Z.-Y. Li et al., Nano Lett. **6**, 765 (2006)
316. Y. Xiong, J. Chen, B. Wiley et al., J. Am. Chem. Soc. **127**, 7332 (2005)
317. Y. Xiong, H. Cai, B.J. Wiley et al., J. Am. Chem. Soc. **129**, 3665 (2007)
318. Y. Xiong, J. Chen, B. Wiley et al., Nano Lett. **5**, 1237 (2005)
319. Y.J. Xiong, J.M. Mclellan, Y.D. Yin et al., Angew. Chem. Int. Ed. **46**, 790 (2007)
320. F. Kim, S. Connor, H. Song et al., Angew. Chem. **116**, 3759 (2004)
321. D. Seo, C.I. Yoo, J.C. Park et al., Angew. Chem. **120**, 775 (2008)
322. H. Song, F. Kim, S. Connor et al., J. Phys. Chem. B **109**, 188 (2005)
323. C. Li, K.L. Shuford, M. Chen et al., ACS nano **2**, 1760 (2008)
324. T.T. Tran, X. Lu, J. Phys. Chem. C **115**, 3638 (2011)
325. X.L. Li, Y. Yang, G.J. Zhou et al., Nanoscale **5**, 4976 (2013)
326. Y. Yang, W. Wang, X. Li et al., Chem. Mater. **25**, 34 (2012)
327. C. Li, L. Sun, Y. Sun et al., Chem. Mater. **25**, 2580 (2013)
328. J.Y. Chen, B. Wiley, Z.Y. Li et al., Adv. Mater. **17**, 2255 (2005)
329. W. Niu, W. Zhang, S. Firdoz et al., J. Am. Chem. Soc. **136**, 3010 (2014)
330. I. Pastoriza-Santos, L.M. Liz-Marzán, Nano Lett. **2**, 903 (2002)

331. Y. Gao, P. Jiang, L. Song et al., J. Cryst. Growth **289**, 376 (2006)
332. G.H. Jeong, M. Kim, Y.W. Lee et al., J. Am. Chem. Soc. **131**, 1672 (2009)
333. X. Huang, Z. Zhao, J. Fan et al., J. Am. Chem. Soc. **133**, 4718 (2011)
334. Y. Dai, X. Mu, Y. Tan et al., J. Am. Chem. Soc. **134**, 7073 (2012)
335. I. Pastoriza-Santos, L.M. Liz-Marzán, Adv. Funct. Mater. **19**, 679 (2009)
336. I. Pastoriza-Santos, L.M. Liz-Marzán, Langmuir **15**, 948 (1999)
337. Y. Chen, X. Gu, C.-G. Nie et al., Chem. Commun. 4181 (2005)
338. D. Wang, Y. Liu, T. You, CrystEngComm **12**, 4028 (2010)
339. M. Chen, B. Wu, J. Yang et al., Adv. Mater. **24**, 862 (2012)
340. C. Cui, L. Gan, M. Neumann et al., J. Am. Chem. Soc. **136**, 4813 (2014)
341. S. Mourdikoudis, L.M. Liz-MarzáN, Chem. Mater. **25**, 1465 (2013)
342. S. Peng, J.M. Mcmahon, G.C. Schatz et al., Proc. Natl. Acad. Sci. U.S.A. **107**, 14530 (2010)
343. S. Sun, C. Murray, D. Weller et al., Science **287**, 1989 (2000)
344. V. Mazumder, M. Chi, K.L. More et al., J. Am. Chem. Soc. **132**, 7848 (2010)
345. C. Wang, D. Van Der Vliet, K.L. More et al., Nano Lett. **11**, 919 (2010)
346. V. Mazumder, S. Sun, J. Am. Chem. Soc. **131**, 4588 (2009)
347. S. Zhang, Ö. Metin, D. Su et al., Angew. Chem. Int. Ed. **52**, 3681 (2013)
348. C. Wang, W. Tian, Y. Ding et al., J. Am. Chem. Soc. **132**, 6524 (2010)
349. S. Zhang, S. Guo, H. Zhu et al., J. Am. Chem. Soc. **134**, 5060 (2012)
350. V. Mazumder, M. Chi, M.N. Mankin et al., Nano Lett. **12**, 1102 (2012)
351. Y. Yu, W. Yang, X. Sun et al., Nano Lett. **14**, 2778 (2014)
352. C.B. Murray, S.H. Sun, H. Doyle et al., MRS Bull. **26**, 985 (2001)
353. Z. Huo, C.-K. Tsung, W. Huang et al., Nano Lett. **8**, 2041 (2008)
354. C. Wang, Y. Hou, J. Kim et al., Angew. Chem. Int. Ed. **46**, 6333 (2007)
355. Z. Niu, Q. Peng, M. Gong et al., Angew. Chem. **123**, 6439 (2011)
356. X. Lu, M.S. Yavuz, H.-Y. Tuan et al., J. Am. Chem. Soc. **130**, 8900 (2008)
357. C. Wang, Y. Hu, C.M. Lieber et al., J. Am. Chem. Soc. **130**, 8902 (2008)
358. Z. Li, J. Tao, X. Lu et al., Nano Lett. **8**, 3052 (2008)
359. H. Feng, Y. Yang, Y. You et al., Chem. Commun. 1984 (2009)
360. N. Pazos-Pérez, D. Baranov, S. Irsen et al., Langmuir **24**, 9855 (2008)
361. S. Guo, D. Li, H. Zhu et al., Angew. Chem. Int. Ed. **52**, 3465 (2013)
362. H. Zhu, S. Zhang, S. Guo et al., J. Am. Chem. Soc. **135**, 7130 (2013)
363. S. Guo, S. Zhang, X. Sun et al., J. Am. Chem. Soc. **133**, 15354 (2011)
364. M. Chen, T. Pica, Y.-B. Jiang et al., J. Am. Chem. Soc. **129**, 6348 (2007)
365. S. Peng, Y. Sun, Chem. Mater. **22**, 6272 (2010)
366. L. Polavarapu, L.M. Liz-Marzán, Nanoscale **5**, 4355 (2013)
367. Y. Ma, W. Li, J. Zeng et al., J. Mater. Chem. **20**, 3586 (2010)
368. J. Zhang, H. Yang, J. Fang et al., Nano Lett. **10**, 638 (2010)
369. J. Zhang, H. Yang, K. Yang et al., Adv. Funct. Mater. **20**, 3727 (2010)
370. H. Yang, J. Zhang, K. Sun et al., Angew. Chem. **122**, 7000 (2010)
371. C. Wang, H. Daimon, T. Onodera et al., Angew. Chem. Int. Ed. **47**, 3588 (2008)
372. R. Loukrakpam, P. Chang, J. Luo et al., Chem. Commun. **46**, 7184 (2010)
373. C. Wang, H. Daimon, Y. Lee et al., J. Am. Chem. Soc. **129**, 6974 (2007)
374. J. Zhang, J. Fang, J. Am. Chem. Soc. **131**, 18543 (2009)
375. Y. Kang, M. Li, Y. Cai et al., J. Am. Chem. Soc. **135**, 2741 (2013)
376. J. Wu, L. Qi, H. You et al., J. Am. Chem. Soc. **134**, 11880 (2012)
377. J. Wu, A. Gross, H. Yang, Nano Lett. **11**, 798 (2011)
378. J. Watt, N. Young, S. Haigh et al., Adv. Mater. **21**, 2288 (2009)
379. J. Watt, S. Cheong, M.F. Toney et al., ACS nano **4**, 396 (2009)
380. J. Ren, R.D. Tilley, J. Am. Chem. Soc. **129**, 3287 (2007)
381. J. Zhang, M.R. Langille, C.A. Mirkin, J. Am. Chem. Soc. **132**, 12502 (2010)
382. M.L. Personick, M.R. Langille, J. Zhang et al., Small **9**, 1947 (2013)
383. J. Zhou, J. An, B. Tang et al., Langmuir **24**, 10407 (2008)
384. B. Pietrobon, V. Kitaev, Chem. Mater. **20**, 5186 (2008)

385. J. Zhang, M.R. Langille, C.A. Mirkin, Nano Lett. **11**, 2495 (2011)
386. R. Keunen, N. Cathcart, V. Kitaev, Nanoscale **6**, 8045 (2014)
387. C. Xue, J.E. Millstone, S. Li et al., Angew. Chem. **119**, 8588 (2007)
388. M.R. Langille, J. Zhang, C.A. Mirkin, Angew. Chem. Int. Ed. **50**, 3543 (2011)
389. C. Xue, G.S. Metraux, J.E. Millstone et al., J. Am. Chem. Soc. **130**, 8337 (2008)
390. P.L. Redmond, X. Wu, L. Brus, J. Phys. Chem. C **111**, 8942 (2007)
391. P.L. Redmond, L.E. Brus, J. Phys. Chem. C **111**, 14849 (2007)
392. C. Xue, C.A. Mirkin, Angew. Chem. **119**, 2082 (2007)
393. J. Zhang, S. Li, J. Wu et al., Angew. Chem. **121**, 7927 (2009)
394. M.R. Langille, J. Zhang, M.L. Personick et al., Science **337**, 954 (2012)
395. J. Xiao, S. Liu, N. Tian et al., J. Am. Chem. Soc. **135**, 18754 (2013)
396. L. Wei, Z.-Y. Zhou, S.-P. Chen et al., Chem. Commun. **49**, 11152 (2013)
397. L. Wei, Y.-J. Fan, N. Tian et al., J. Phys. Chem. C **116**, 2040 (2011)
398. N. Tian, Z.-Y. Zhou, S.-G. Sun, Chem . Commun. 1502 (2009)
399. Y.-X. Chen, S.-P. Chen, Z.-Y. Zhou et al., J. Am. Chem. Soc. **131**, 10860 (2009)
400. L. Zhang, W. Niu, G. Xu, Nano Today **7**, 586 (2012)
401. Z.Y. Jiang, Q. Kuang, Z.X. Xie et al., Adv. Funct. Mater. **20**, 3634 (2010)
402. Z.W. Quan, Y.X. Wang, J.Y. Fang, Acc. Chem. Res. **46**, 191 (2013)
403. Y. Li, Y. Jiang, M. Chen et al., Chem. Commun. **48**, 9531 (2012)
404. N.F. Yu, N. Tian, Z.Y. Zhou et al., Angew. Chem. Int. Ed. **126**, 5197 (2014)
405. Y.-J. Deng, N. Tian, Z.-Y. Zhou et al., Chem. Sci. **3**, 1157 (2012)
406. N. Tian, Z.-Y. Zhou, N.-F. Yu et al., J. Am. Chem. Soc. **132**, 7580 (2010)